
nature
Science
NEW ENGLAND JOURNAL of MEDICINE
PHYSICAL REVIEW LETTERS
Cell
jbc
the journal of biological chemistry
PNAS
ASTROPHYSICAL JOURNAL
наукові публікації

наукова інформація повинна бути у публічному доступі

- **може бути оцінена**
- **приносить користь**

*ta*kiltum of the diagonal *from which 1 is* torn out so that the width *comes up*	ÍB.SI$_8$ of the width	ÍB.SI$_8$ of the diagonal
(1) *59 00* 15	1 59	2 49
(1) *56 56* 58 14 56 15 (1) *56 56* 58 14 [50 06] 15	56 07	3 12 01 [1 20 25]
(1) *55 07* 41 15 33 45	1 16 41	1 50 49
(1) 5*3* 10 29 32 52 16	3 31 49	5 09 01
(1) 48 54 01 40	1 05	1 37
(1) 47 06 41 40	5 19	8 01
(1) 43 11 56 28 26 40	38 11	59 01
(1) 41 33 59 03 45 (1) 41 33 [45 14] 03 45	13 19	20 49
(1) 38 33 36 36	9 01 [8] 01	12 49
(1) 35 10 02 28 27 24 26 40	1 22 41	2 16 01
(1) 33 45	45	1 15
(1) 29 21 54 02 15	27 59	48 49
(1) 27 00 03 45	7 12 01 [2 41]	4 49
(1) 25 48 51 35 06 40	29 31	53 49
(1) 23 13 46 40	56 56 [28] (alt.)	53 [1 46] 53 (alt.)

числа Піфагора

шкільне завдання

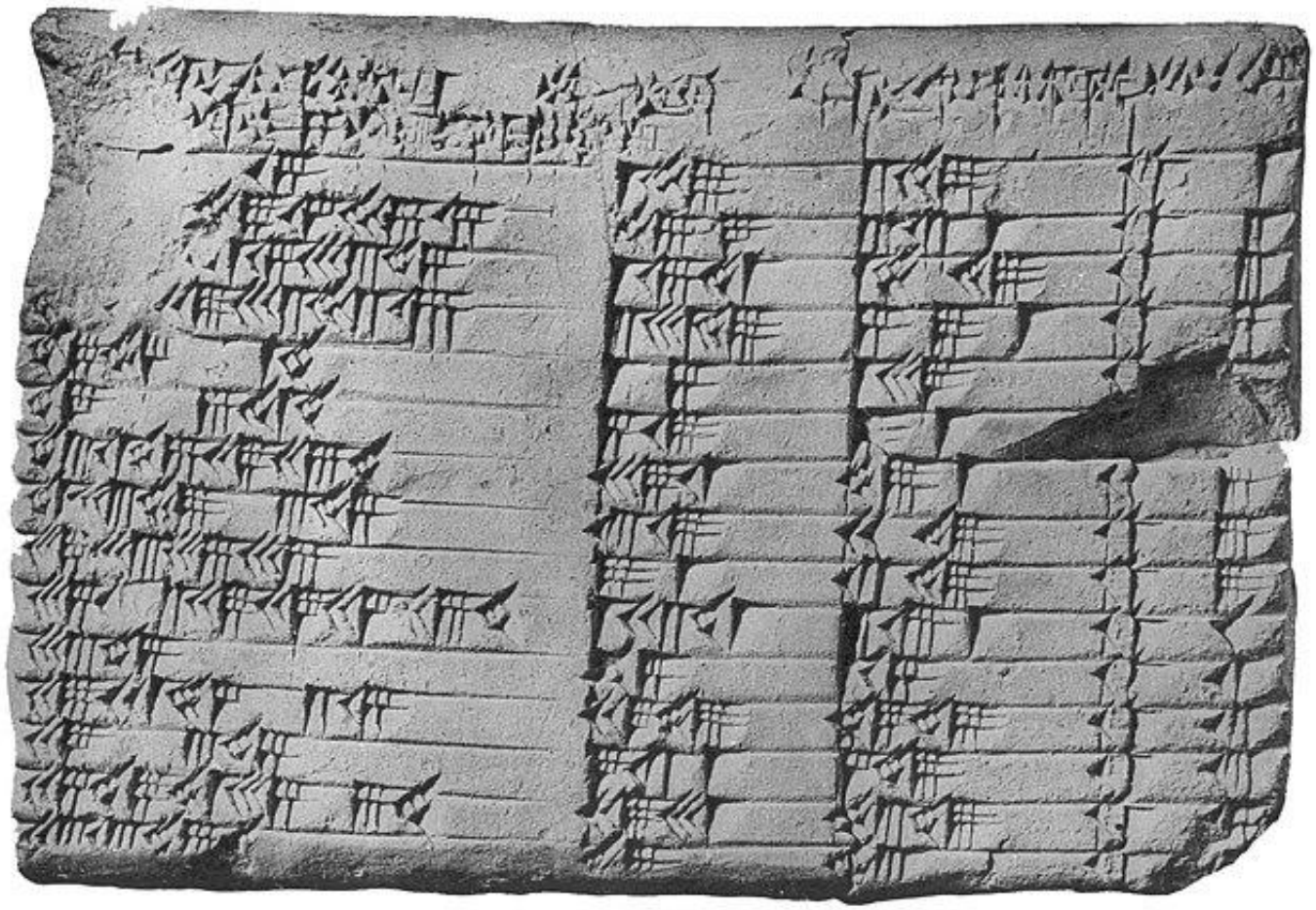

теорема Піфагора

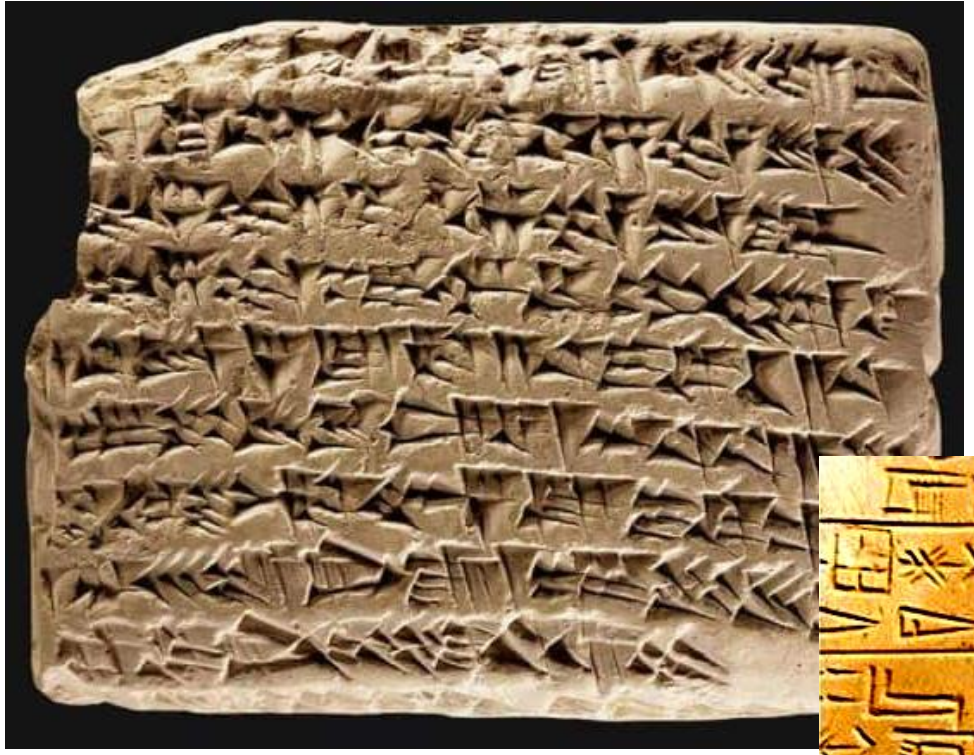

рецептура

приготування **мила**

I.Newton, 1687

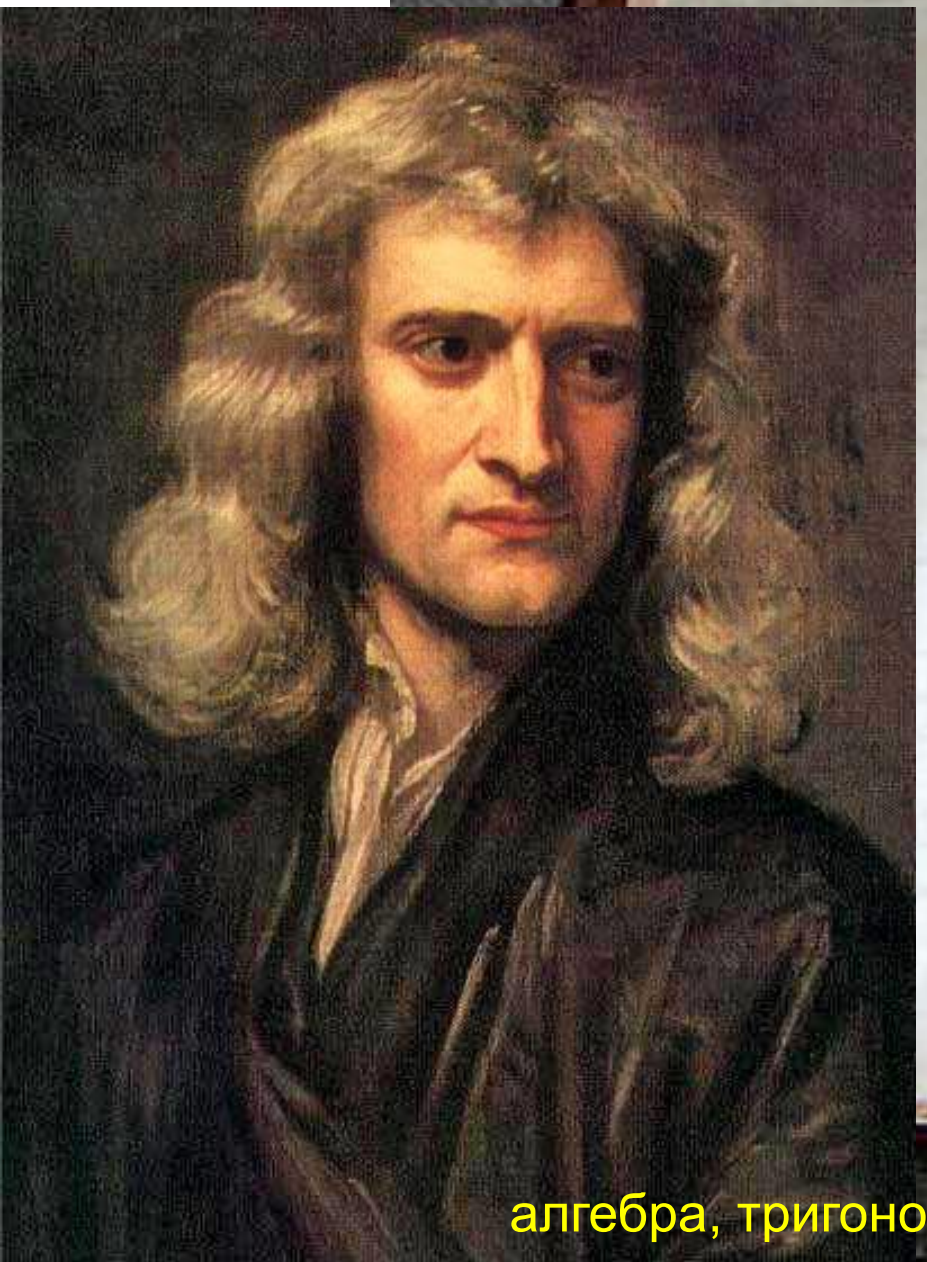

PHILOSOPHIÆ
NATURALIS
PRINCIPIA
MATHEMATICA

Auctore J.S. NEWTONO, Trin. Coll. Cantab. Soc. Mathesos
Professore Lucasiano, & Societatis Regalis Sodali.

IMPRIMATUR.
S. PEPYS, Reg. Soc. PRÆSES.
Julii 5. 1686.

LONDINI,
Jussu Societatis Regiæ ac Typis Josephi Streater. Prostat apud
plures Bibliopolas. Anno MDCLXXXVII.

алгебра, тригонометрія – диф.числення: астрономія, артилерія, маятник, двигун

Charles Darwin
1859

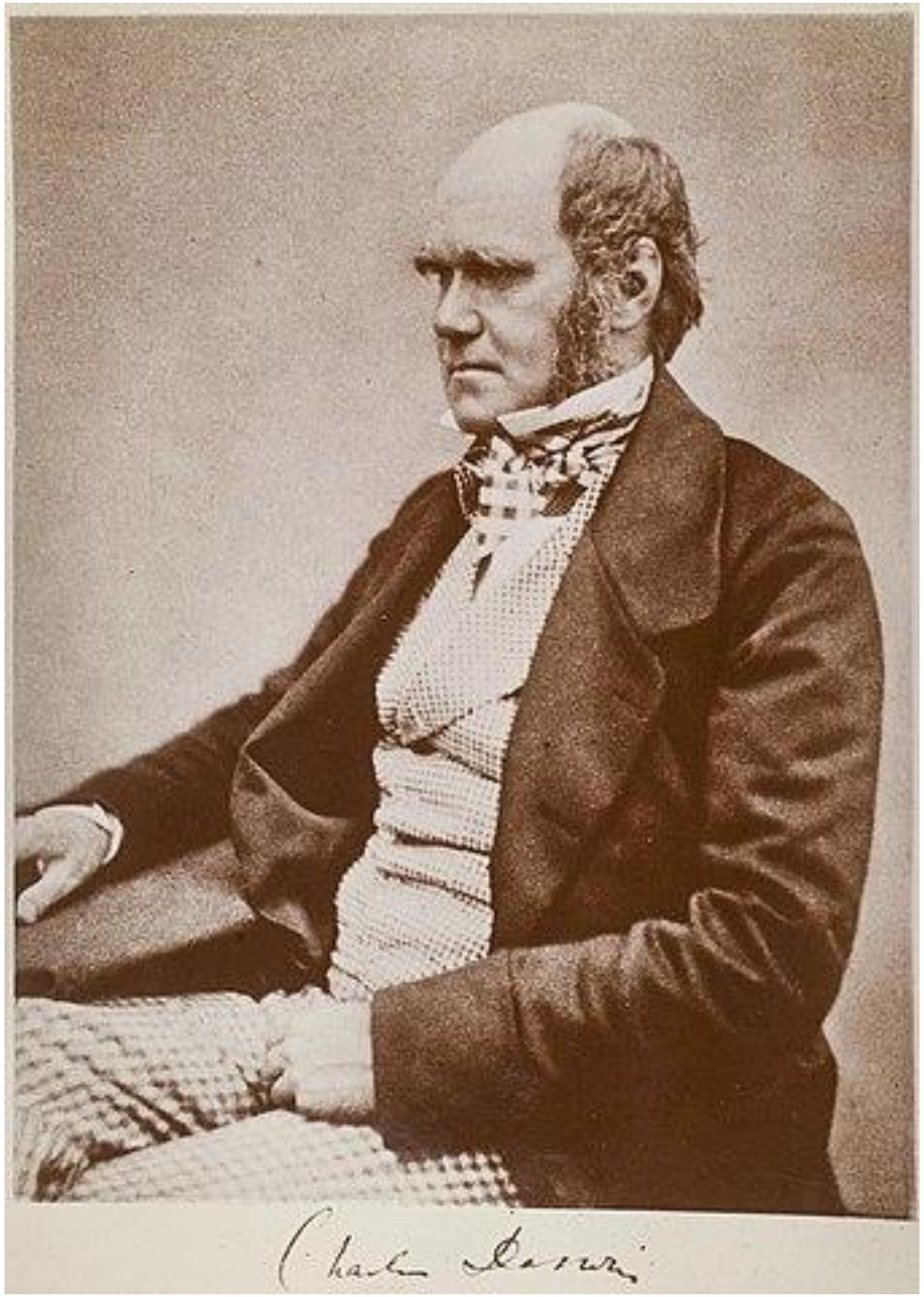

ON

THE ORIGIN OF SPECIES

BY MEANS OF NATURAL SELECTION,

OR THE

PRESERVATION OF FAVOURED RACES IN THE STRUGGLE FOR LIFE.

By CHARLES DARWIN, M.A.,

FELLOW OF THE ROYAL, GEOLOGICAL, LINNÆAN, ETC., SOCIETIES;
AUTHOR OF 'JOURNAL OF RESEARCHES DURING H. M. S. BEAGLE'S VOYAGE ROUND THE WORLD.'

LONDON:
JOHN MURRAY, ALBEMARLE STREET.
1859.

Friedrich Wöhler
1877

Das *Jodür* $C^6H^{13}J$ ist eine bei 179°,5 siedende Flüssigkeit von 1,4115 spec. Gewicht bei 17°,5.

Secundäre Hexylalkohole.

2. **Methylbutylcarbinol** (*β-Hexylalkohol*) $CH^3.CH^2.CH^2.CH^2.CH\begin{matrix}OH\\CH^3\end{matrix}$. Bei der Destillation von Mannit mit concentrirter Jodwasserstoffsäure entsteht das bei 167°,5 siedende Jodür dieses Alkohols. — Der *β*-Hexyl-Aethyläther $C^6H^{13}.O.C^2H^5$ (bei 131° siedende Flüssigkeit von 0,7865 spec. Gewicht bei 0°) entsteht durch Einwirkung von Zinkäthyl auf Aethylchloräther (s. secund. Butylalkohol S. 79); dieser wird durch Erhitzen mit Jodwasserstoffsäure in Jodäthyl und *β*-Hexyljodür gespalten. Aus dem Jodür wird durch Erhitzen mit Silberoxyd und Wasser der Alkohol erhalten. — Bei 137° siedende Flüssigkeit von 0,8327 spec. Gewicht bei 0°. In Wasser fast unlöslich. Verhält sich gegen Schwefelsäure ähnlich wie das Amylenhydrat. Liefert bei der Oxydation Kohlensäure, Essigsäure und Buttersäure, als intermediäres Product Methyl-Butylketon.

Das *Chlorür* desselben Alkohols ($C^6H^{13}Cl$, Siedepunct 125—126°) bildet sich zugleich mit dem Chlorür des primären Alkohols bei der Einwirkung von Chlor auf normales Hexan.

3. **Aethylpropylcarbinol** $CH^3.CH^2CH^2.CH\begin{matrix}OH\\CH^2.CH^3\end{matrix}$. Durch Einwirkung von Wasserstoff im Entstehungszustand auf Aethylpropylketon. — Farblose, in Wasser kaum lösliche Flüssigkeit. Siedepunct 134—135°. Spec. Gewicht 0,834 bei 0°. Liefert bei der Oxydation zuerst Aethylpropylketon, *dann* Propionsäure.

Das *Jodür* $C^6H^{13}J$ siedet bei 164—166°.

4. **Pinakolylalkohol** $(CH^3)^3C.CH\begin{matrix}OH\\CH^3\end{matrix}$. Entsteht bei der Einwirkung von Wasserstoff im Entstehungszustand auf

Oct 1877

WÖHLER'S GRUNDRISS

DER

ORGANISCHEN CHEMIE

VON

DR. RUDOLPH FITTIG,
O. PROFESSOR DER CHEMIE AN DER UNIVERSITÄT STRASSBURG.

ZEHNTE UMGEARBEITETE AUFLAGE.

LEIPZIG,
VERLAG VON DUNCKER & HUMBLOT.
1877.

ANNALEN

DER

CHEMIE UND PHARMACIE.

LXIX. Bandes drittes Heft.

Untersuchungen über die Elektrolyse organischer Verbindungen;

von Dr. *H. Kolbe.*

Erste Abhandlung.

Die vorliegende Untersuchung schliefst sich an einige frühere Beobachtungen *) über die oxydirende Wirkung des im Kreise des galvanischen Stromes sich ausscheidenden Sauerstoffs, welche er im Status nascens auf die Chlorkohlenunterschwefelsäure, Salzsäure **) u. a. ausübt. Die Leichtigkeit, womit besonders erstere Säure, welche sonst auf nasssem Wege den stärksten oxydirenden Agentien widersteht, durch den elektrolysirten Sauerstoff zerlegt wird, läfst darin eins der allerkräftigsten Oxy-

*) Observations on the oxydizing power of Oxygen, when disengaged

in der Auflösung des valeriansauren Kali's dreierlei Erscheinungen hervor:

1) die Zerlegung der Säure selbst in Valyl und Kohlensäure,

$$\underbrace{HO \,.\, (C_8\ H_9)\ C_2\ O_3}_{\text{Valeriansäure.}} + O = \underbrace{C_8\ H_9}_{\text{Valyl.}} + 2\ CO_2 + HO$$

2) die Zersetzung des Valyls in Ditetrylgas und Wasser,

$$\underbrace{C_8\ H_9}_{\text{Valyl.}} + O = 2\ \underbrace{C_4\ H_4}_{\text{Ditetryl.}} + HO$$

3) eine directe Oxydation des Valyls zu Valyloxyd, welches letztere im Entstehungsmomente sich dann mit einem Atom Valeriansäure verbindet,

$$\underbrace{C_8\ H_9}_{\text{Valyl.}} + O + \underbrace{(C_8\ H_9)\ C_2\ O_3}_{\text{Valeriansäure.}} = C_8\ H_9\ \text{vale}$$

Die beiden letzten Processe scheinen abhängig von einander vor sich zu gehen, nicht gelungen, genau die Umstände zu ermitteln, Bildung des einen oder des anderen Produkts günstigen.

Elektrolyse der Essigsäure.

Die grofse Analogie der Säuren der Essigsäurereihe berechtigt zu der Vermuthung, dafs die Essigsäure an Pole des galvanischen Stromes eine ähnliche

H.Kolbe, 1849

August Beer

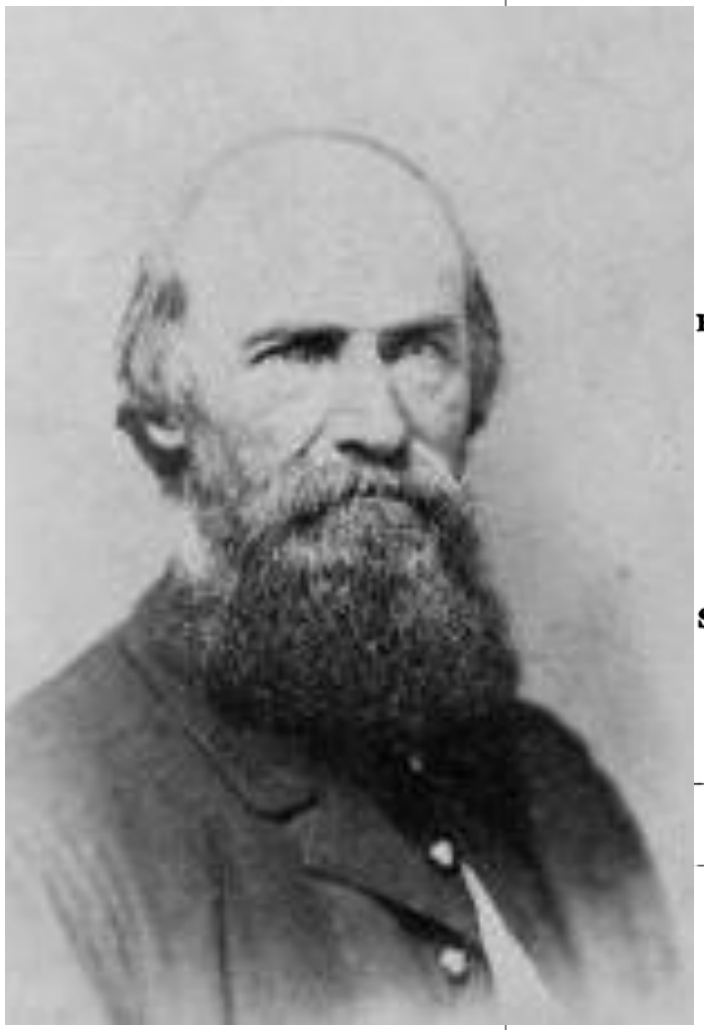

ANNALEN

DER

PHYSIK

UND

CHEMIE.

HERAUSGEGEBEN ZU BERLIN

VON

J. C. POGGENDORFF.

SECHS UND ACHTZIGSTER BAND.

GANZEN FOLGE HUNDERT UND ~~DREI~~ 2 UND SECHSZIGSTER.

NEBST DREI KUPFERTAFELN.

LEIPZIG, 1852.

VERLAG VON JOHANN AMBROSIUS BARTH.

III. *Bestimmung der Absorption des rothen Lichts in farbigen Flüssigkeiten; von Beer in Bonn.*

Oftmals schon ist die Absorption des Lichtes beim Durchstrahlen gefärbter Substanzen zum Gegenstande des Versuchs gemacht worden; man richtete hiebei jedoch immer nur das Augenmerk auf die relative Schwächung der verschiedenen Farben oder, bei krystallisirten Körpern, auf die Beziehung zwischen der Absorption und der Polarisations-Richtung. Ueber die absolute Gröfse der Absorption, welche irgend ein bestimmter Lichtstrahl bei der Fortpflanzung in einem adiaphanen Mittel erleidet, liegt meines Wissens Nichts vor. Nur mit Rücksicht hierauf theile ich in diesem Aufsatze eine Reihe von Maafsbestimmungen der absorbirenden Kraft mit. Andererseits nämlich entgeht mir die Unvollständigkeit meiner Bestimmungen keineswegs. Sie beziehen sich nur auf rothes Licht, wie es von einem dunkelrothen Glase geliefert wird. Wünschenswerth aber wäre es, jedesmal die Absorption von wenigstens allen Hauptfarben des Spectrums zu erhalten. Dieſs kann jedoch nur mit viel complicirteren Einrichtungen ereicht werden, als mir zu Gebote stehen. Ein Gleiches ist zu bemerken in Betreff des Umstandes, dafs ich nicht mit Sonnenlichte, sondern mit Lampenlichte operirte. Ich sah mich deshalb genöthigt, meist nur geringe Dicken oder verdünnte Lösungen der färbenden Salze (denn auf solche habe ich mich beschränkt) dem Versuche zu unterwerfen; hierdurch wird aber der Werth der numerischen Ergeb-

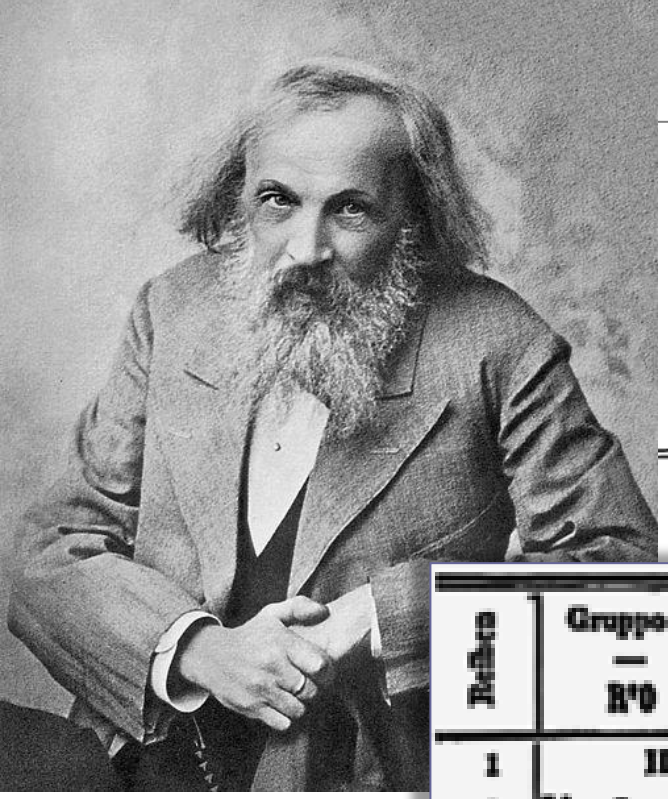

1869

ЖУРНАЛЪ
РУССКАГО ХИМИЧЕСКАГО ОБЩЕСТВА.
ТОМЪ I.

Соотношеніе свойствъ съ атомнымъ вѣсомъ элементовъ.

Д. Менделѣева.

Систематическое распредѣленіе элементовъ подвергалось въ исторіи нашей науки многимъ разнообразнымъ превратностямъ. Наиболѣе распространенное раздѣленіе ихъ на *металлы* и *металлоиды* опирается какъ на физическія различія, замѣчаемыя между многими простыми тѣлами, такъ и на различія въ характерѣ ихъ словъ и соотвѣтственныхъ имъ соединеній. Но то, что казалось при первомъ знакомствѣ съ предметомъ, яснымъ и абсолютнымъ, то при потеряло свое значе- что одинъ элементъ остояніи металлоида, ъ опираться на раз- основныхъ и кислот- ельства сколько либо овными и кислотными ходныхъ, куда напр шьяка, золота, пла- ъ. Притомъ аналогія , ванадій, сурьма и теллура съ селеномъ нона съ оловомъ, не раздѣленіи простыхъ ми. Изслѣдованія ме- что сѣра, фосфоръ и ого же разряда, какъ еще болѣе яснымъ го заключ нія. ованы на *отношеніи*

Ряды	Gruppe I. — R^1O	Gruppe II. — RO	Gruppe III. — R^2O^3	Gruppe IV. RH^4 RO^2	Gruppe V. RH^3 R^2O^5	Gruppe VI. RH^2 RO^3	Gruppe VII. RH R^2O^7	Gruppe VIII. — RO^4
1	H=1							
2	Li=7	Be=9,4	B=11	C=12	N=14	O=16	F=19	
3	Na=23	Mg=24	Al=27,5	Si=28	P=31	S=32	Cl=35,5	
4	K=39	Ca=40	—=44	Ti=48	V=51	Cr=52	Mn=55	Fe=56, Co=59, Ni=59, Cu=63.
5	(Cu=63)	Zn=65	—=68	—=72	As=75	Se=78	Br=80	
6	Rb=85	Sr=87	?Yt=88	Zr=90	Nb=94	Mo=96	—=100	Ru=104, Rh=104, Pd=106, Ag=108.
7	(Ag=108)	Cd=112	In=113	Sn=118	Sb=122	Te=125	J=127	
8	Cs=133	Ba=137	?Di=138	?Ce=140	—	—	—	— — — —
9	(—)	—	—	—	—	—	—	
10	—	—	?Er=178	?La=180	Ta=182	W=184	—	Os=195, Ir=197, Pt=198, Au=199.
11	(Au=199)	Hg=200	Tl=204	Pb=207	Bi=208	—	—	
12	—	—	—	Th=231	—	U=240	—	— — — —

г. Министру Народнаго Просвѣщенія, на утвержденіе

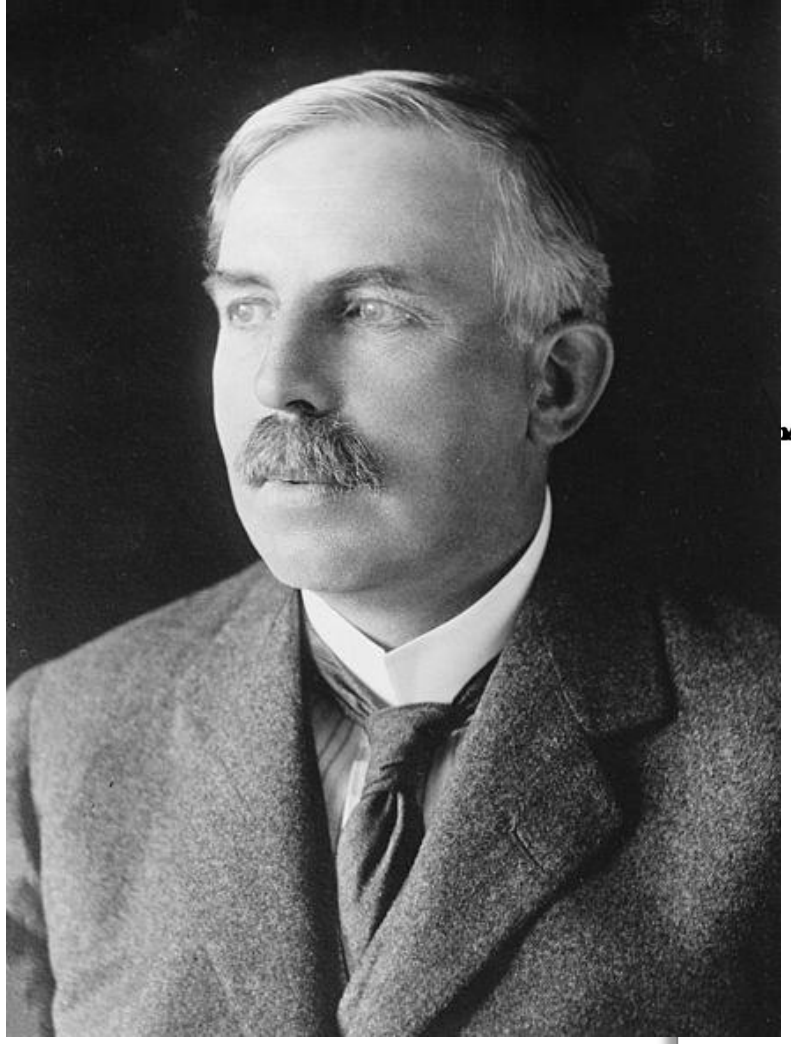

Ernest Rutherford

RADIO-ACTIVITY

BY

E. RUTHERFORD, D.Sc., F.R.S., F.R.S.C.
MACDONALD PROFESSOR OF PHYSICS, McGILL UNIVERSITY, MONTREAL

SECOND EDITION

CAMBRIDGE
AT THE UNIVERSITY PRESS
1905

RADIOACTIVE SUBSTANCES AND THEIR RADIATIONS

BY

E. RUTHERFORD, D.Sc., Ph.D., LL.D., F.R.S.
NOBEL LAUREATE
LANGWORTHY PROFESSOR OF PHYSICS, UNIVERSITY OF MANCHESTER

Cambridge:
at the University Press
1913

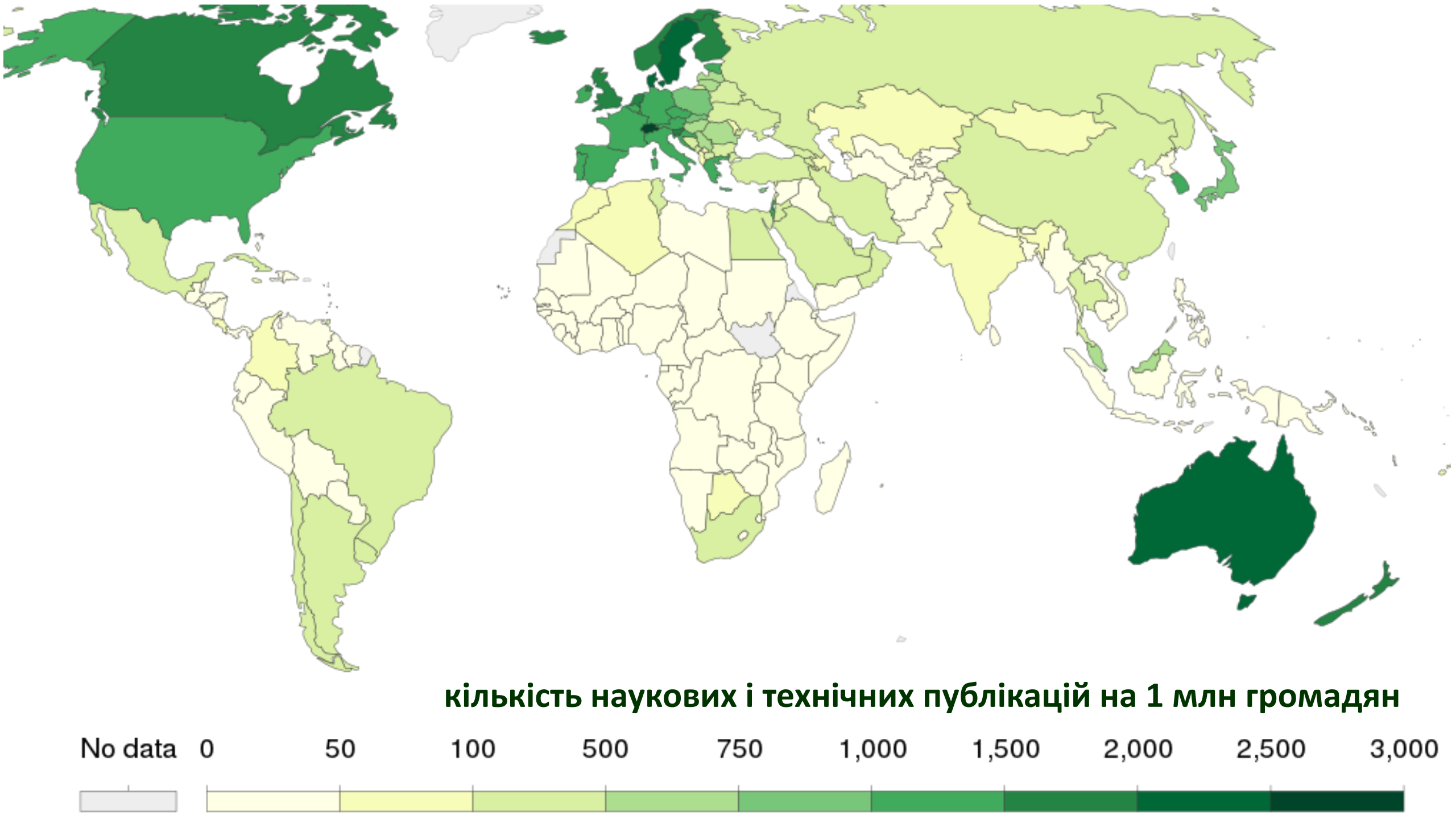
кількість наукових і технічних публікацій на 1 млн громадян
No data
0
50
100
500
750
1,000
1,500
2,000
2,500
3,000

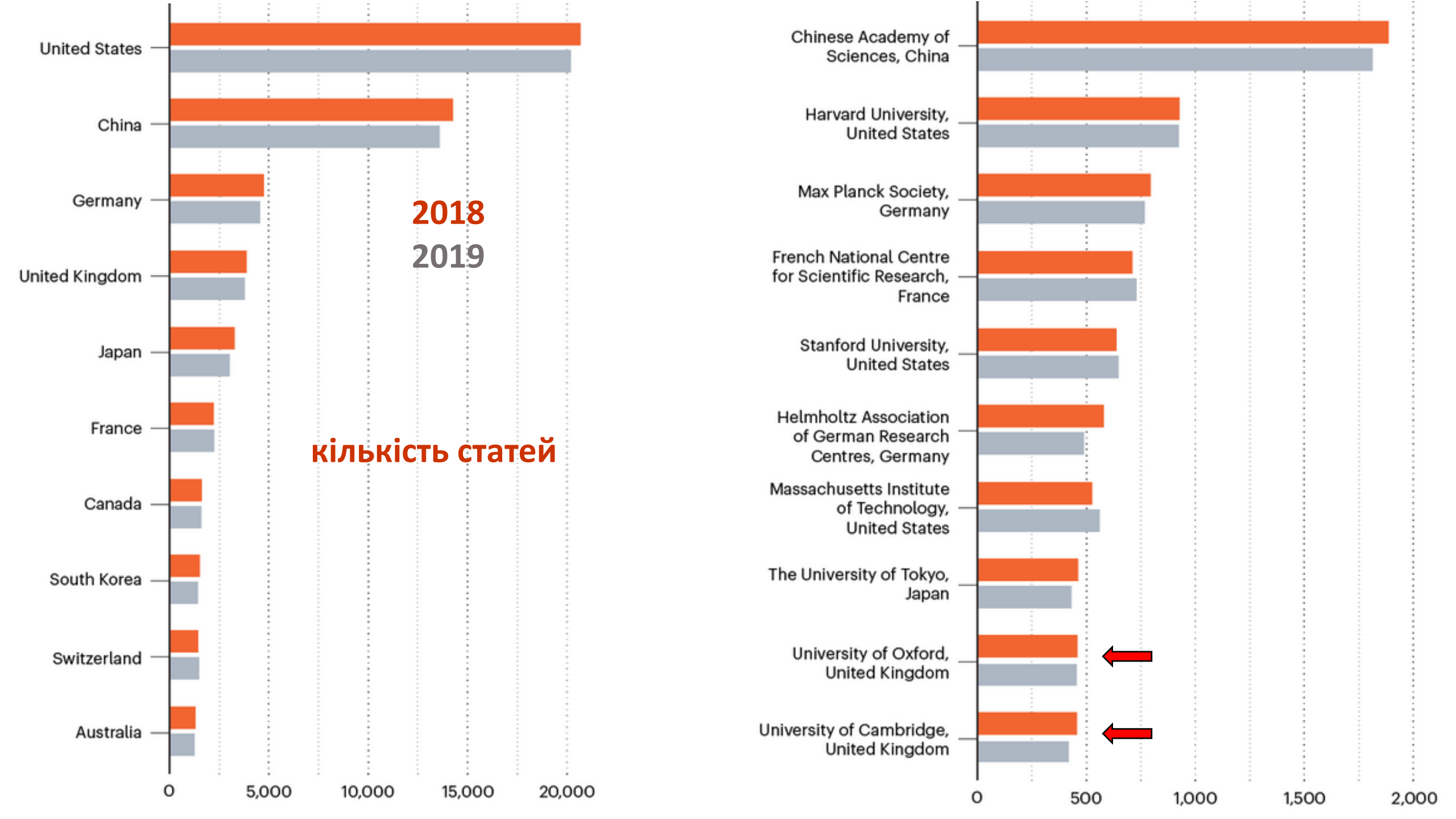
United States
China
Germany
United Kingdom
Japan
France
Canada
South Korea
Switzerland
Australia
0
5,000
10,000
15,000
20,000
2018
2019
кількість статей
Chinese Academy of Sciences, China
Harvard University, United States
Max Planck Society, Germany
French National Centre for Scientific Research, France
Stanford University, United States
Helmholtz Association of German Research Centres, Germany
Massachusetts Institute of Technology, United States
The University of Tokyo, Japan
University of Oxford, United Kingdom
University of Cambridge, United Kingdom
0
500
1,000
1,500
2,000

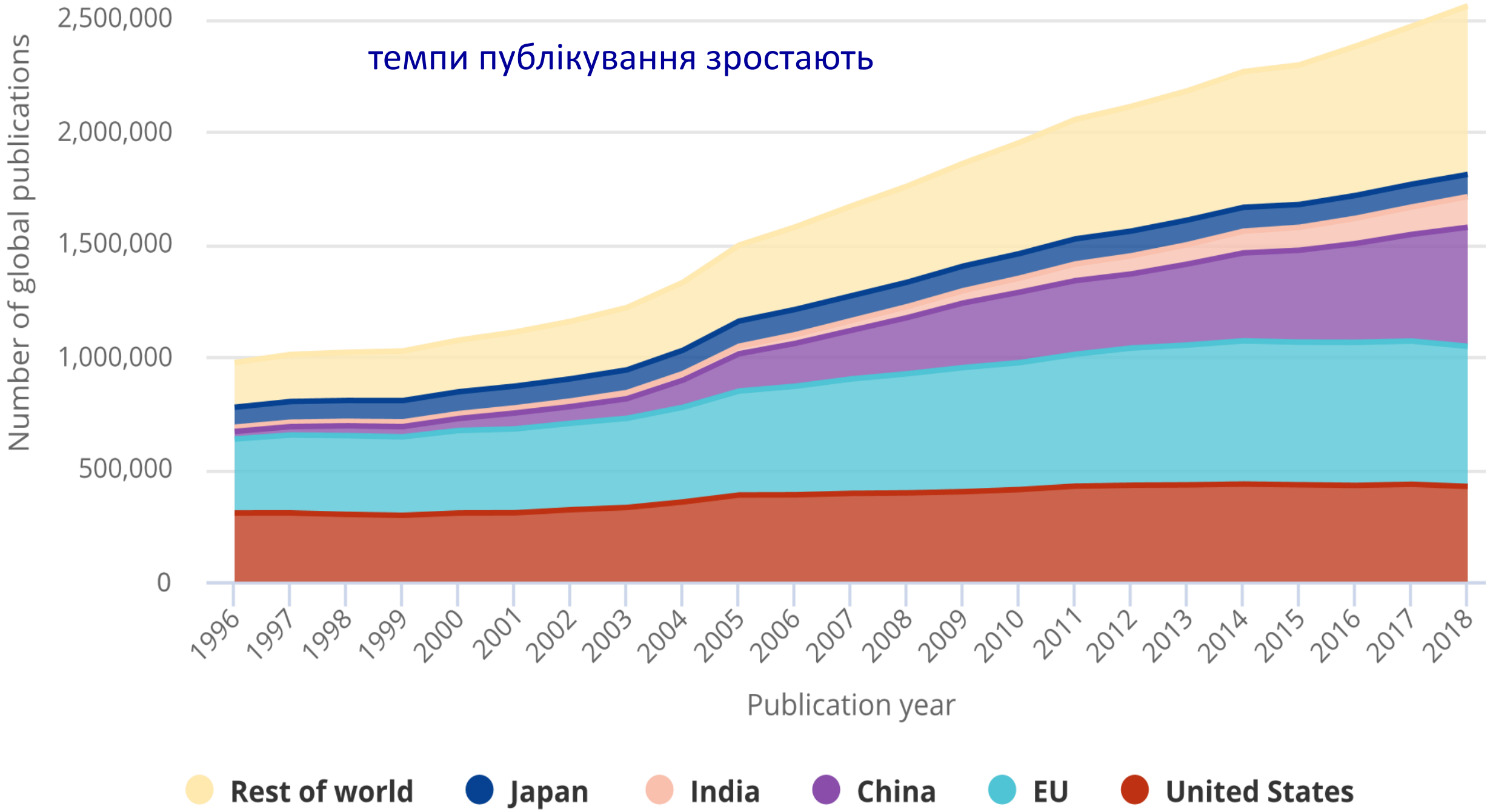
темпи публікування зростають
Number of global publications
2,500,000
2,000,000
1,500,000
1,000,000
500,000
0
1996
1997
1998
1999
2000
2001
2002
2003
2004
2005
2006
2007
2008
2009
2010
2011
2012
2013
2014
2015
2016
2017
2018
Publication year
Rest of world
Japan
India
China
EU
United States

частка публікацій змінюється

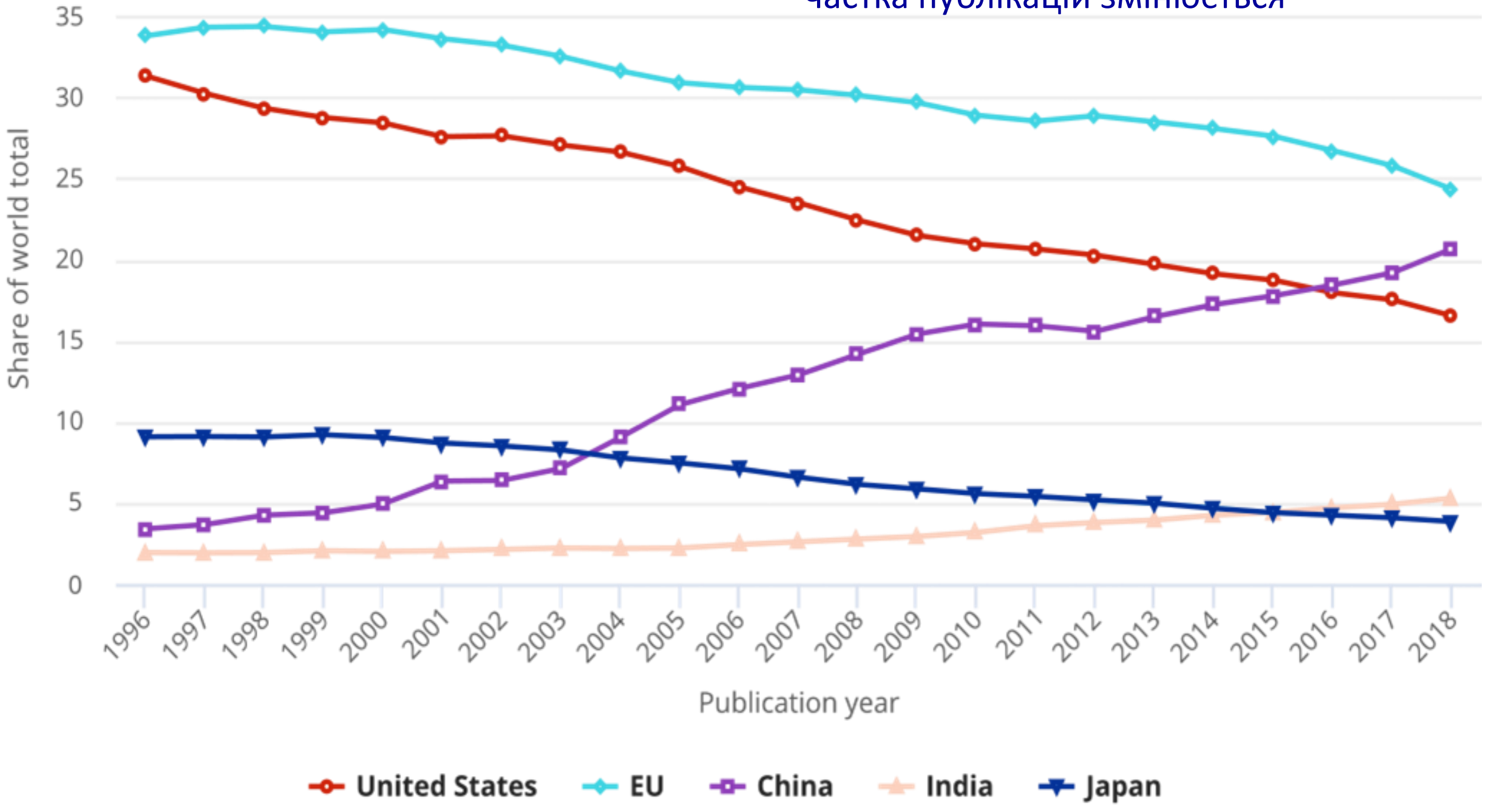

частка публікацій змінюється

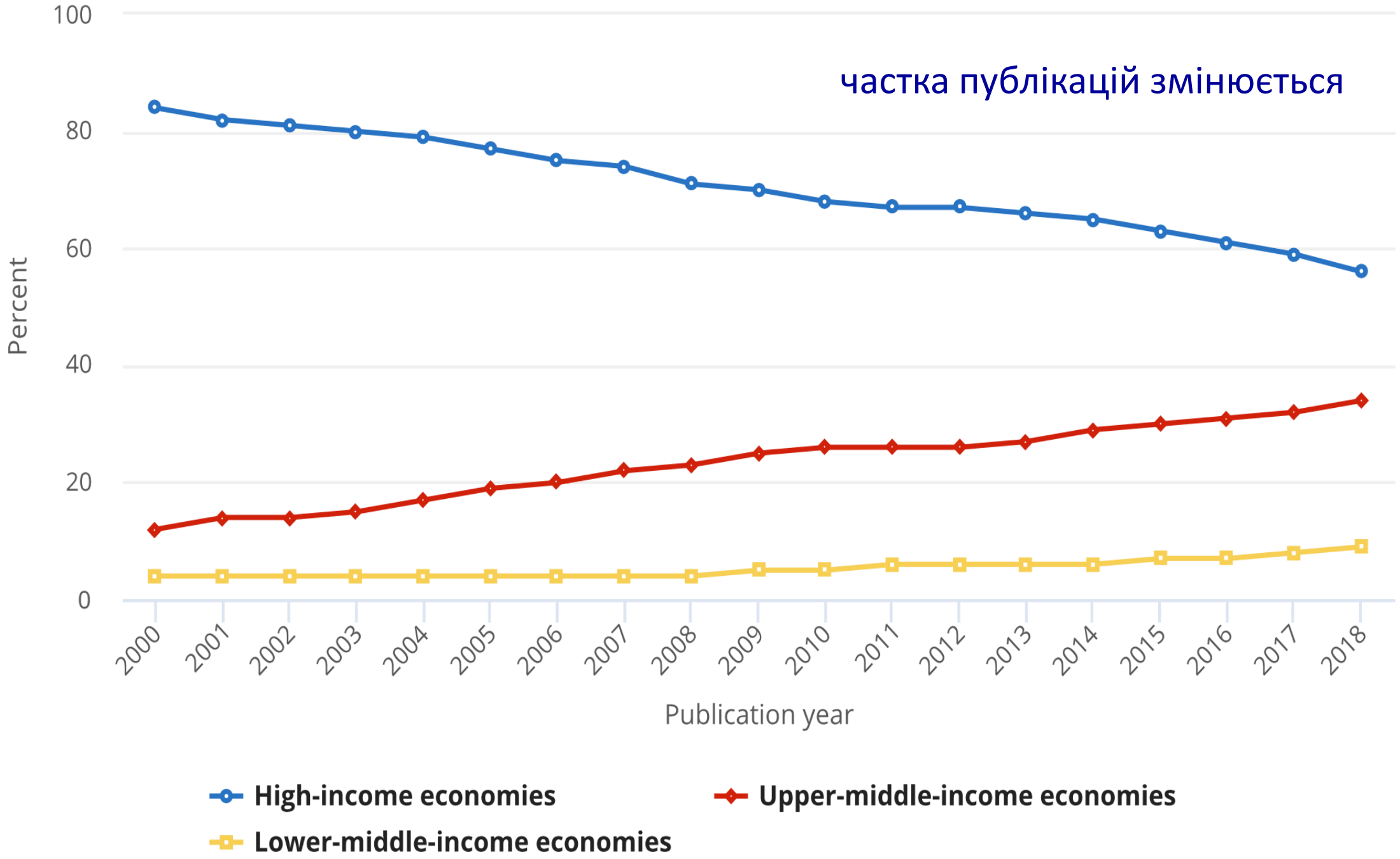

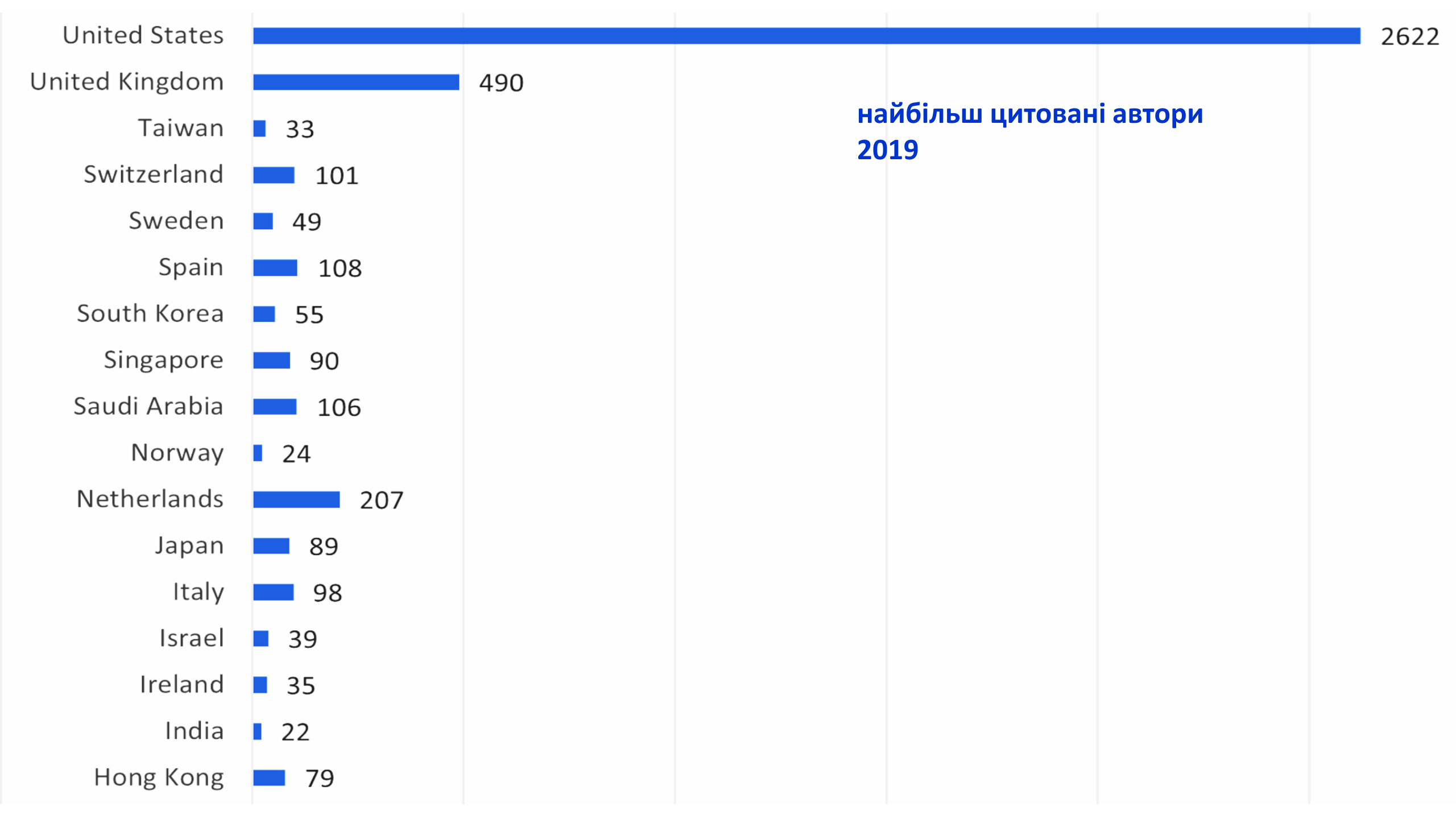
United States 2622
United Kingdom 490
Taiwan 33
Switzerland 101
Sweden 49
Spain 108
South Korea 55
Singapore 90
Saudi Arabia 106
Norway 24
Netherlands 207
Japan 89
Italy 98
Israel 39
Ireland 35
India 22
Hong Kong 79
найбільш цитовані автори
2019

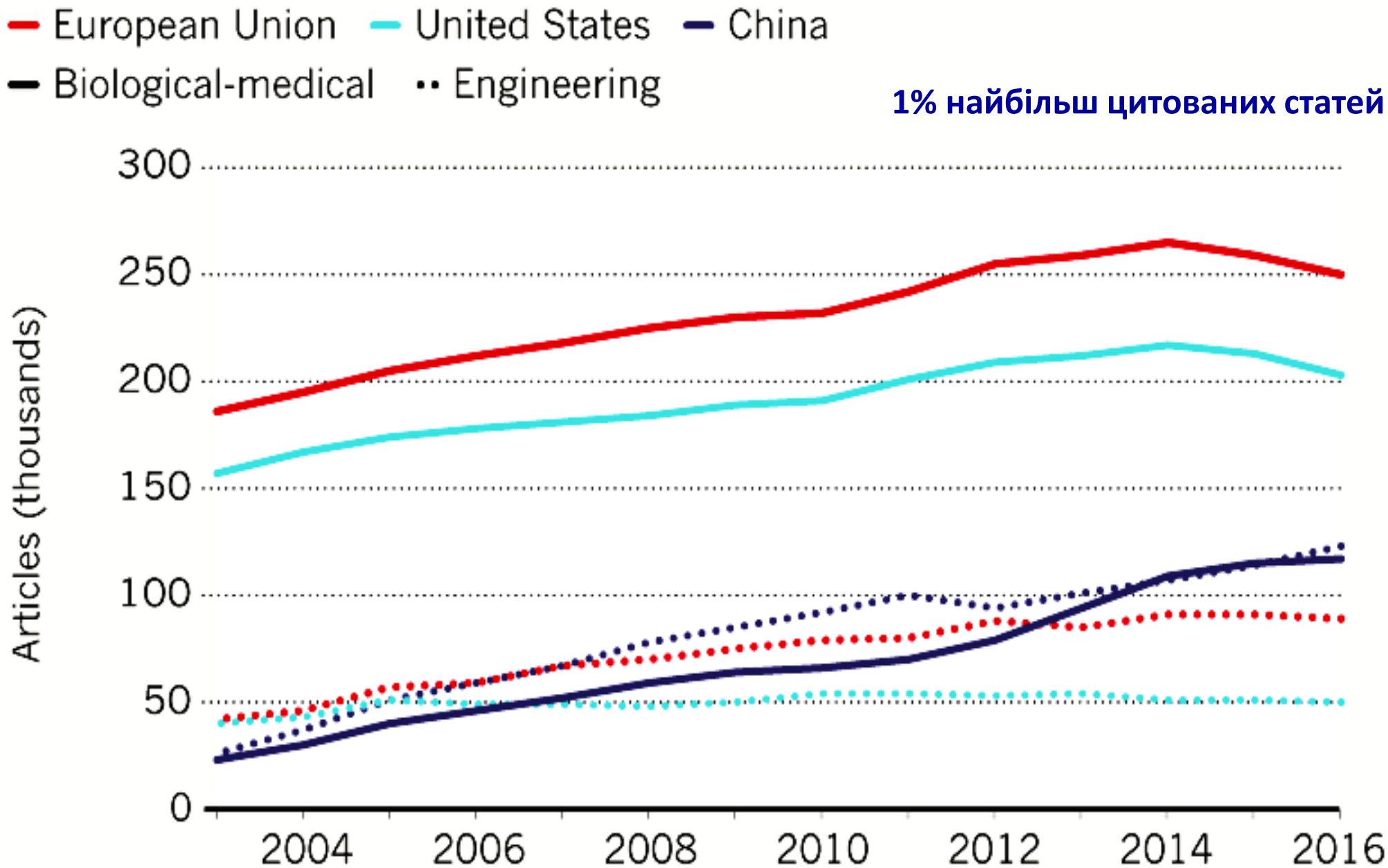
European Union
United States
China
Biological-medical
Engineering
1% найбільш цитованих статей
Articles (thousands)
300
250
200
150
100
50
0
2004
2006
2008
2010
2012
2014
2016

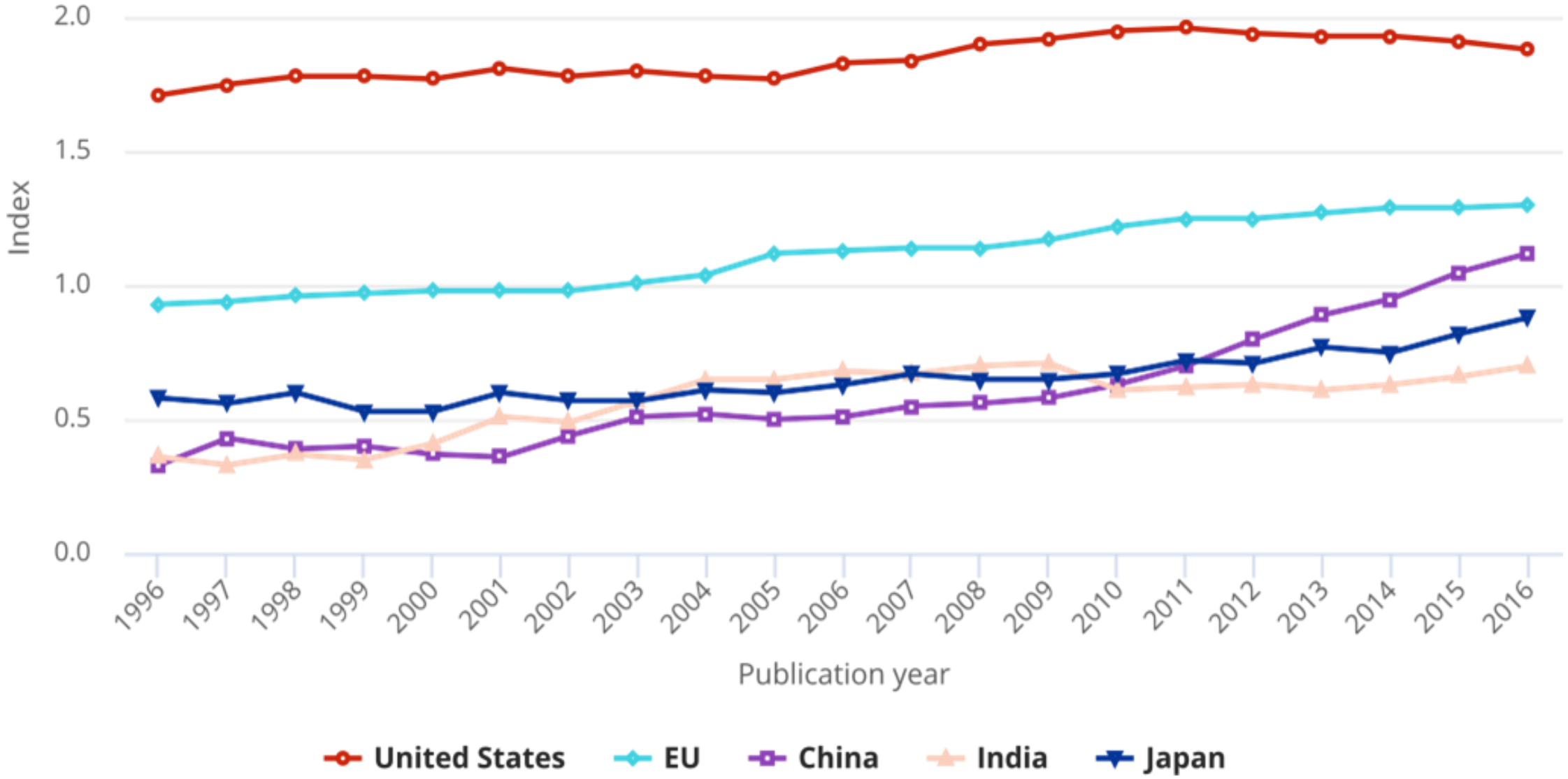

The share of articles in the top 1% is computed as follows: *Sx* = *HCPx*/*Px*, where *Sx* is the share of output from country *x* in the top 1% most-cited articles; *HCPx* is the number of articles from country *x* that are among the top 1% of most-cited articles ; and *Px* is the total number of papers from country *x*.
The world average stands at 1.00 for each year

Highly cited scientific papers country rankings

1998-2000 (average) No. of papers		2008-2010 (average) No. of papers		2018-2020 (average) No. of papers	
1. U.S.	30,710	1. U.S.	36,910	1. China	46,352
2. Britain	6,071	2. China	9,011	2. U.S.	36,680
3. Germany	4,991	3. Britain	7,420	3. Britain	8,772
4. Japan	4,369	4. Germany	6,477	4. Germany	7,246
5. France	3,609	5. France	4,568	5. Italy	6,073
6. Canada	2,842	6. Japan	4,369	6. Australia	5,099
7. Italy	2,128	7. Canada	4,078	7. India	4,926
8. Netherlands	1,814	8. Italy	3,450	8. Canada	4,509
9. Australia	1,687	9. Australia	2,941	9. France	4,231
10. Spain	1,398	10. Spain	2,903	10. Spain	3,845
⋮				11. South Korea	3,798
13. China	1,217			12. Japan	3,780

Source: Education ministry

Note: Number of papers in top 10% of most-cited papers in each research field

публікування

показує **політику держав**

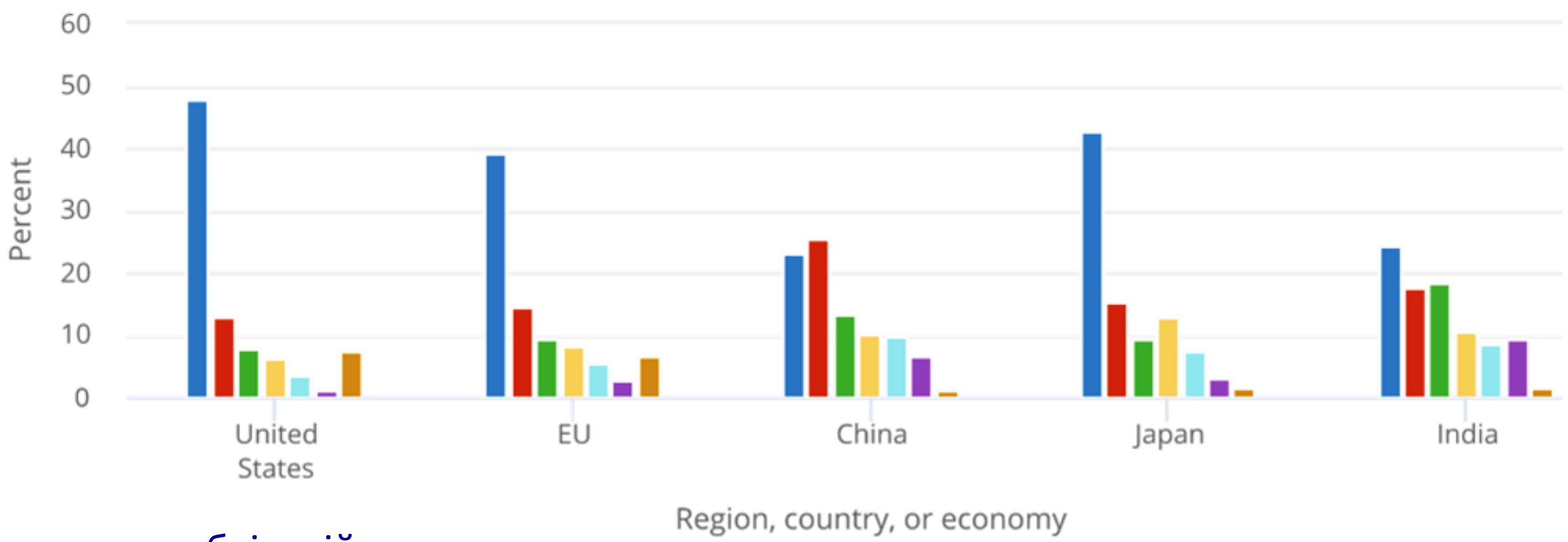

частка публікацій
за тематикою
показує **політику держави**

- **Health sciences and biological and biomedical sciences**
- **Engineering**
- **Computer and information sciences**
- **Physics**
- **Chemistry**
- **Materials science**
- **Social sciences**

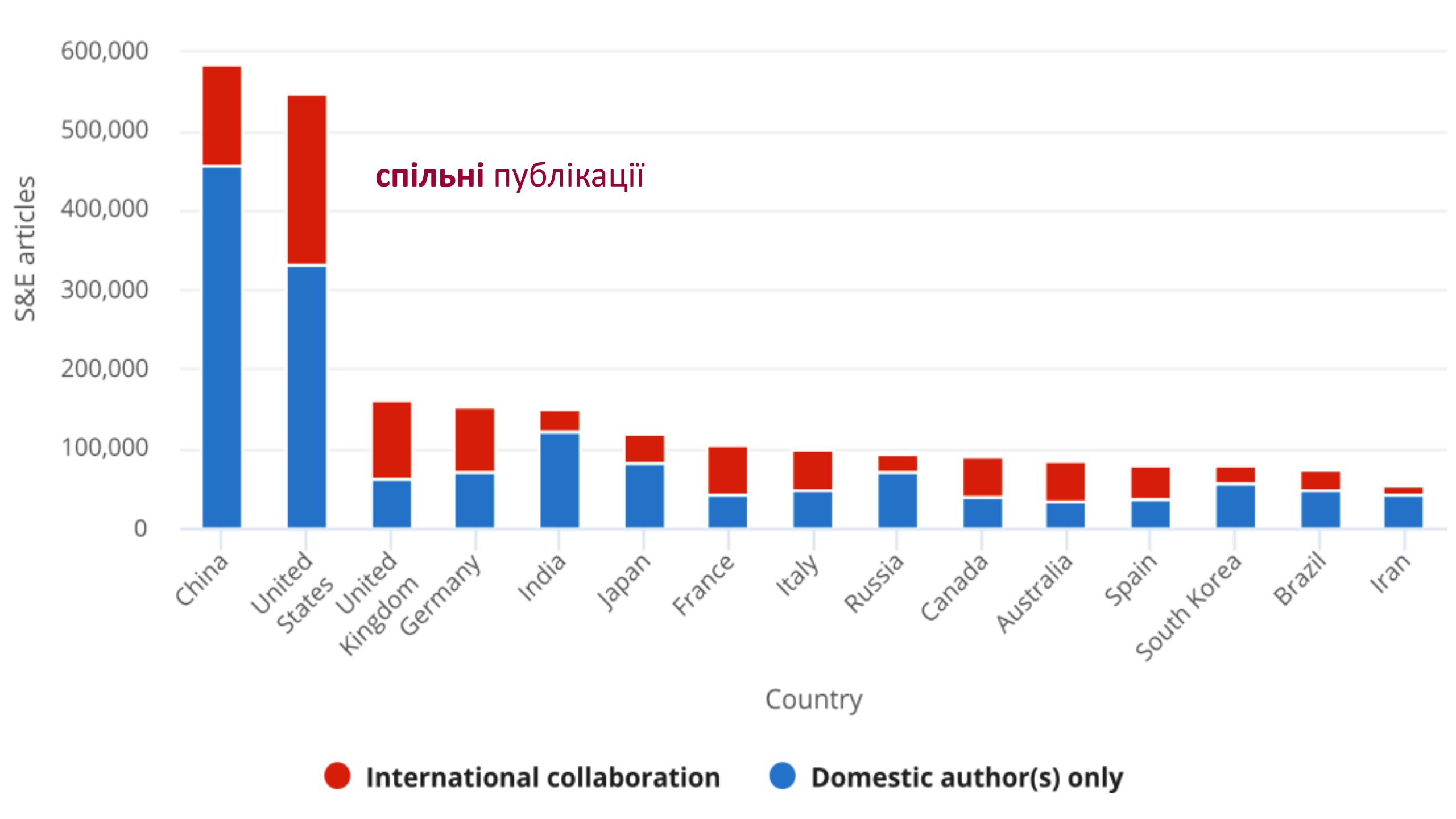
600,000
500,000
400,000
300,000
200,000
100,000
0
S&E articles
спільні публікації
China
United States
United Kingdom
Germany
India
Japan
France
Italy
Russia
Canada
Australia
Spain
South Korea
Brazil
Iran
Country
International collaboration
Domestic author(s) only

Photocatalytic degradation of dyes using rutile TiO_2 synthesized by reverse micelle and low temperature methods: real-time monitoring of the degradation kinetics

Tetiana Tatarchuk [a, b], Nazarii Danyliuk [a], Alexander Shyichuk [c, d], Wojciech Macyk [e], Mu. Naushad [f]

[a] Educational and Scientific Center of Material Science and Nanotechnology, Vasyl Stefanyk Precarpathian National University, Ivano-Frankivsk 76018, Ukraine

[b] School of Science and Technology, Glocal University, Saharanpur, India

[c] Department of Chemistry, Vasyl Stefanyk Precarpathian National University, 57 Shevchenko Street, 76018 Ivano-Frankivsk, Ukraine

[d] Faculty of Chemical Technology and Engineering, Politechnika Bydgoska im. Jana i Jędrzeja Śniadeckich, 3, Seminaryjna str., 85-326, Bydgoszcz, Poland

[e] Faculty of Chemistry, Jagiellonian University, ul. Gronostajowa 2, 30-387 Kraków, Poland

[f] Department of Chemistry, College of Science, King Saud University, P.O. Box 2455, Riyadh-11451, Saudi Arabia

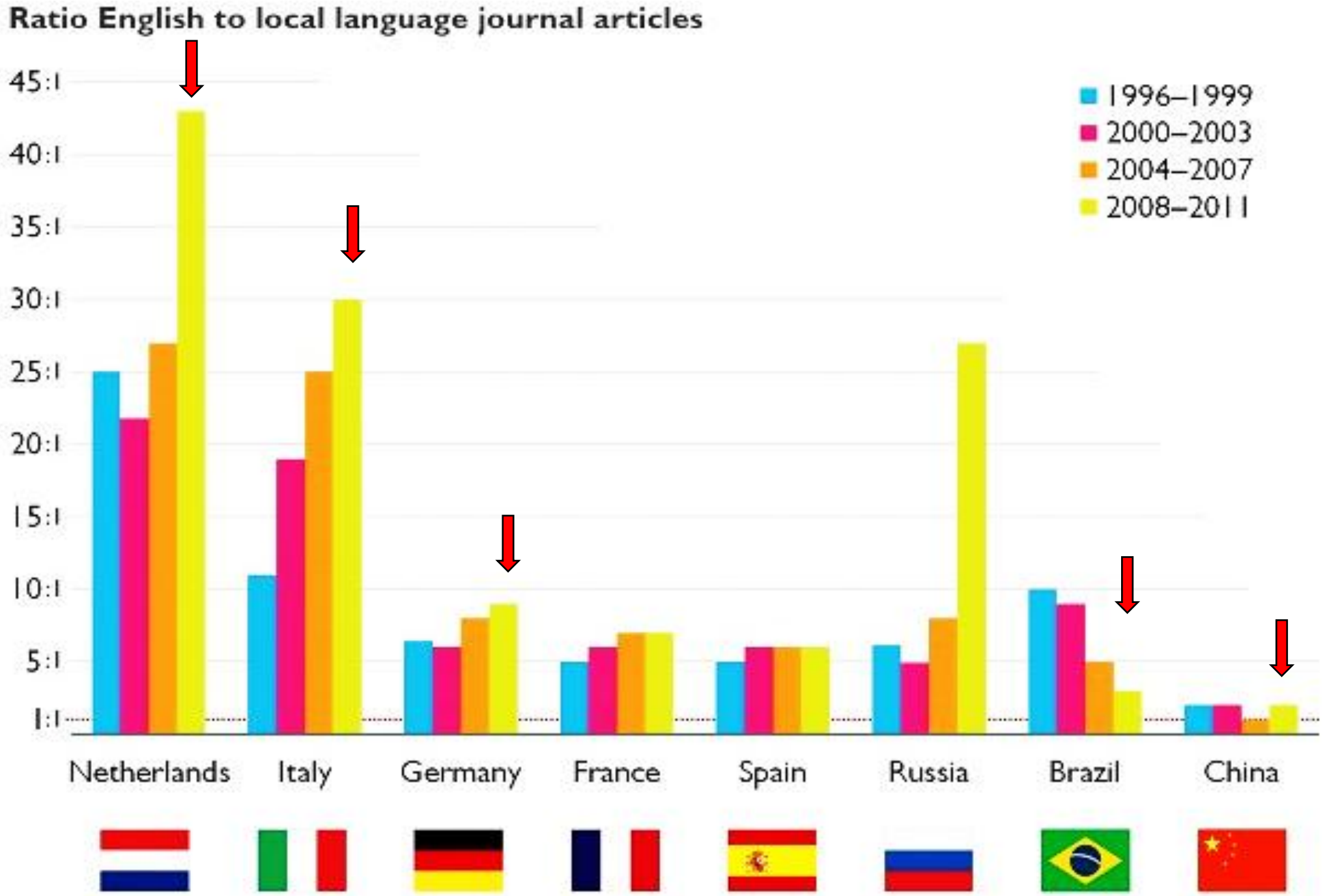
Ratio English to local language journal articles
45:1
40:1
35:1
30:1
25:1
20:1
15:1
10:1
5:1
1:1
1996–1999
2000–2003
2004–2007
2008–2011
Netherlands
Italy
Germany
France
Spain
Russia
Brazil
China

Journal of Alloys and Compounds 819 (2020) 152945

Contents lists available at ScienceDirect

Journal of Alloys and Compounds

journal homepage: http://www.elsevier.com/locate/jalcom

Synthesis, morphology, crystallite size and adsorption properties of nanostructured Mg–Zn ferrites with enhanced porous structure

Tetiana Tatarchuk [a, b, *], Mariana Myslin [c], Ivan Mironyuk [a], Mohamed Bououdina [d], Antoni T. Pędziwiatr [e], Renata Gargula [e], Bogdan F. Bogacz [e], Piotr Kurzydło [e]

[a] Department of Chemistry, Vasyl Stefanyk Precarpathian National University, 57 Shevchenko Street, 76018, Ivano-Frankivsk, Ukraine
[b] Faculty of Chemical Technology and Engineering, UTP University of Science and Technology, 3, Seminaryjna str., 85-326, Bydgoszcz, Poland
[c] Educational and Scientific Center of Material Science and Nanotechnology, Vasyl Stefanyk Precarpathian National University, Ivano-Frankivsk, 76018, Ukraine
[d] Department of Physics, College of Science, University of Bahrain, PO Box 32038, Bahrain
[e] Smoluchowski Institute of Physics, Jagiellonian University, ul. Łojasiewicza 11, 30-348, Kraków, Poland

ARTICLE INFO

Article history:
Received 19 August 2019
Received in revised form
3 November 2019

ABSTRACT

Mg–Zn ferrites with porous cavity structure were produced by sol-gel auto-combustion method utilizing a new mixture of DL-alanine and urea as an organic fuel-reductant. The influence of non-magnetic Zn ions content on the structural, morphological and adsorption characteristics of Mg–Zn NPs has been inves-

Table 1
Lattice parameter (a_{exp}), density (d_{exp}), porosity (P), surface area

x Zn^{2+}	a_{exp}, nm	Cation distribution
0.0	0.8377	$(Mg^{2+}_{0.1}Fe^{3+}_{0.9})_A[Mg^{2+}_{0.9}Fe^{3+}_{1.1}]_B O_4$
0.2	0.8381	$(Mg^{2+}_{0.08}Zn^{2+}_{0.02}Fe^{3+}_{0.90})_A[Mg^{2+}_{0.72}$
0.4	0.8405	$(Mg^{2+}_{0.06}Zn^{2+}_{0.04}Fe^{3+}_{0.90})_A[Mg^{2+}_{0.54}$
0.6	0.8418	$(Mg^{2+}_{0.04}Zn^{2+}_{0.06}Fe^{3+}_{0.90})_A[Mg^{2+}_{0.36}$
0.8	0.8427	$(Mg^{2+}_{0.02}Zn^{2+}_{0.08}Fe^{3+}_{0.90})_A[Mg^{2+}_{0.18}$
1.0	0.8435	$(Zn^{2+}_{0.1}Fe^{3+}_{0.9})_A[Fe^{3+}_{1.1}]_B O_4$

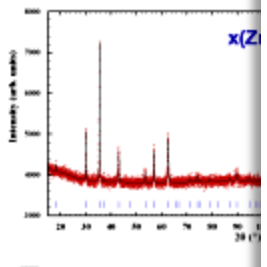

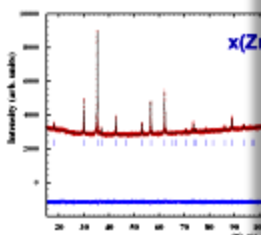

Fig. 2. Kleinveil refinem

where m_1 is the weight of the sample in air, m_2 is th
sample in the organic solvent (ethanol) and d_{EtOH} i
organic solvent (density of ethanol is equal 0.7893 g
The bulk density d_{exp} of $Mg_{1-x}Zn_xFe_2O_4$ system de
from 3.760 to 3.294 g/cm^3 with the increase in Zn c

The porosity of the ferrite materials has been c
the following expression [15]:

$$P = \left(1 - \frac{d_{exp}}{d_{XRD}}\right) \times 100\%$$

It is found that the porosity increases significa
38% with Zn content for $Mg_{1-x}Zn_xFe_2O_4$ system, as sh

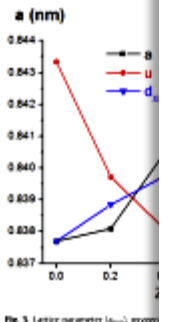

Fig. 3. Lattice parameter (a_{exp}) oxygen

The modified Scherer formula can be written as fo

$$\ln\beta = \ln\left(\frac{k\cdot\lambda}{D_{SM}\cdot\cos\theta}\right) = \ln\left(\frac{k\cdot\lambda}{D_{SM}}\right) + \ln\left(\frac{1}{\cos\theta}\right)$$

where D_{SM} is average crystallite size, k is a constant (
is line broadening in radians (FWHM), δ is Bragg ang
wavelength (λ = 0.1540 nm). The intercept of linear plo
vs. lnβ gives the crystallite size [in nanometers] [inter
D_{SM}]. Since the Bragg peak width is an integration of
instrument-dependent effects, the line broadening h
mated using next formula (6) [48]:

$$\beta = \sqrt{\left[\left\langle\delta^2_{measured}\right\rangle - \left\langle\delta^2_{instrumental}\right\rangle\right]}$$

The crystallite size is also estimated using William
H) method [45]:

$$\beta\cdot\cos\theta = \frac{k\cdot\lambda}{D_{WH}} + 4\varepsilon\cdot\sin\theta$$

where ε is the microstrain. The linear plot ($\beta\cos\theta$ vs.
calculate the crystallite size (in nanometers) (intercep
and microstrain (slope = ε).

The third model, which has been used for the calcu
crystallite size, is the size-strain plot (SSP) method.
benefits in comparison with previous methods –

Table 2
The crystallite sizes (D), microstrain (ε) and dislocation density (δ)
method (W-H) and size-strain plot method (SSP).

x (Zn^{2+})	SH method		W-H
	D_{SM}, nm	δ	D_{W-H}
0.0	25	0.0008	36
0.2	30	0.0011	31
0.4	34	0.0008	45
0.6	42	0.006	48
0.8	38	0.007	50
1.0	30	0.0011	30

Table 3
The values of Mössbauer hyperfine interaction parameters of ($Mg_{1-x}Zn_xFe$
number which follows indicates the number of Zn atoms in the nearest neig
–percentage contributions to the total spectrum, z – partition coefficient, δ

Sample	Component	H_{hf} [T] ($\pm$0.03)	IS [mm/s] ($\pm$0.02)	QS [mm/s] ($\pm$
x = 0.0	Sextet A	48.53	0.26	−0.016
	Sextet B	46.55	0.38	0.026
x = 0.2	Sextet A	48.18	0.28	−0.018
	Sextet B_0	48.27	0.31	−0.008
	Sextet B_1	45.52	0.31	−0.021
	Sextet B_2	41.77	0.31	−0.034
	Sextet B_3	38.02	0.31	−0.047
	Sextet B_4	34.25	0.31	−0.060
x = 0.4	Sextet A	48.27	0.27	−0.013
	Sextet B_0	53.01	0.32	−0.004
	Sextet B_1	48.64	0.32	−0.005
	Sextet B_2	42.27	0.32	−0.006
	Sextet B_3	37.90	0.32	−0.018
	Sextet B_4	33.53	0.32	−0.015
	Sextet B_5	28.16	0.32	−0.020
x = 0.6	Sextet A	48.08	0.25	−0.018
	Sextet B_0	49.08	0.31	0.090
	Sextet B_1	42.18	0.31	0.037
	Sextet B_2	35.28	0.31	0.024
	Sextet B_3	28.38	0.31	0.011
	Sextet B_4	21.48	0.31	−0.002
	Sextet B_5	14.58	0.31	−0.015
x = 0.8	Doublet A	-	0.33	0.32
	Doublet B	-	0.33	0.32
x = 1.0	Doublet A	-	0.33	0.23
	Doublet B	-	0.33	0.23
	Doublet A	-	0.34	0.23
	Doublet B	-	0.34	0.23

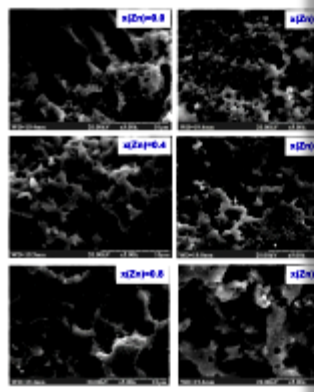

Fig. 7. Scanning electron microscopy of magnesium-zinc ferrites.

3d shell, through contact with the nucleus make a po
contribution to the magnetic field H_{hf}, thus reducing the neg
contribution of the internal electrons. The magnitudes o

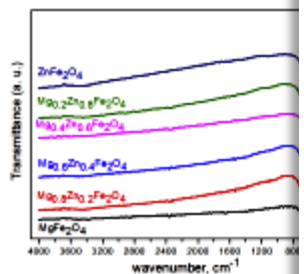

Fig. 9. The IR-spectra of magnesium-zinc ferrites.

Table 4
The infrared absorption bands and force constants for $Mg_{1-x}Zn_xFe_2O_4$ sa

x (Zn^{2+})	ν_1 (cm^{-1})	ν_2 (cm^{-1})	K_A = 10^5 (dyn/cm^2)	K_B = 10^5 (
0	595.23	419.57	2.22	1.39
0.2	588.14	481.00	2.28	1.31
0.4	558.46	358.53	2.30	0.90
0.6	557.17	382.40	2.28	0.94
0.8	548.43	378.86	2.24	1.84
1.0	541.67	382.75	2.20	1.87

characteristic of chemical bonds in the spinel structure.
constants K_T and K_O for tetrahedral and octahedral site
tively for Mg–Zn ferrites have been calculated from ν_1 and
using the following formula (10) [15]:

$$K = 4\pi^2c^2\nu^2\mu,$$

where c is the light velocity (c = 2.99·10^8 m/s); ν_i is IR peak
(cm^{-1}); μ is the reduced mass of the vibrating atoms, kg:

$$\mu = [15.999m_1)(m_i + 15.999)]\cdot[1.6605\cdot10^{-27}],$$

where m_i is the weighted average atomic mass of th

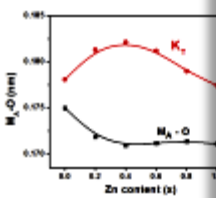

Fig. 10. The correlations between the (a) struc

centers with the same energy, that is satisfy the boundary appli
cability conditions of the Langmuir model with a monomolecular
covering. It should be noted that the Langmuir and Freundlich
constants K_L and K_F testify about the affinity of CR dye molecules to
the ferrites surface. As can be seen from Table 5, the constants K_L
and K_F increase with increasing Zn content reaching maximum
values for $Mg_{0.2}Zn_{0.8}Fe_2O_4$ (K_L = 0.68, K_F = 14.69) and $ZnFe_2O_4$
(K_L = 1.80, K_F = 22.90) samples, thereby confirming the concept of a
much greater affinity of CR dye molecules to the surface of Zn-rich
samples rather than to the surface of the Mg-rich samples.

Another criterion for evaluating the adsorptive capacity of a
sorbent is a dimensionless magnitude called equilibrium parameter
R_L, which is defined as:

$$R_L = \frac{1}{1 + KC_i} \quad (15)$$

where K is the adsorption equilibrium constant of Langmuir model;
C_i is the initial concentration of the adsorbate (CR) in solution. The
calculated R_L values according to the Langmuir model for the
studied ferrite samples are in the range 0.006–0.153 ($0 < R_L < 1$),
signifying that the samples are favorable for anionic dye adsorption
[Table 5]. A lowest R_L value for sample with x (Zn) = 1.0 in com-
parison with other samples indicates that CR adsorption on its
surface is the most favorable, which is confirmed by experimental
data: the adsorption capacity 31 mg/g of $ZnFe_2O_4$ which is few
times higher than for other ferrites (Table 5).

The nature of the adsorption forces is quite different. For this
purpose the Dubinin-Radushkevich model indicates the nature of
the adsorbate-adsorbent bonding and can be used to calculate the
average free adsorption energy: $E = (2K_{DR})^{-0.5}$. The value of K_{DR} is
very important, because it can be used to assess the nature of the
interaction forces between CR dye molecules with active surface
centers. It will also reflects whether the adsorption of CR dye
molecules onto the ferrites surface is a physical process or it has a
chemical nature. It is considered that if the value of E lies between 8
and 16 kJ/mol, then the adsorption process is caused by the ion
exchange; if the value of E is less than 8 kJ/mol, then the adsorption
occurs by physical phenomena and if the value of E is more than
16 kJ/mol, then it is dominated by chemical processes.
Fig. 11d shows the linear graphs of ln(q_e) versus ε^2 for CR adsorption

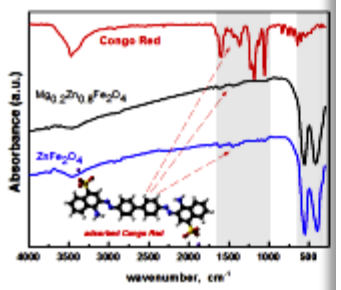

Fig. 12. IR spectra of (a) Congo red dye; (b) $Mg_{0.2}Zn_{0.8}Fe_2O_4$ and (c) $ZnFe_2O_4$ sample
after Congo Red dye adsorption.

at 293 K for the studied samples. The slope of the straight lines

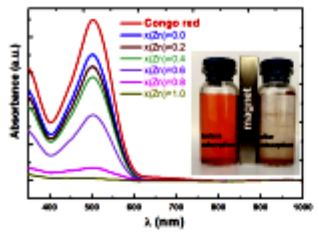

Fig. 14. The absorption spectra of Congo-Red residual concentration after adsorption onto magnetic magnesium-zinc ferrite nanoparticles. In the inset the corresponding photographs are shown. CR solution with concentration of 25 mg/L before and after adsorption onto $Mg_{0.2}Zn_{0.8}Fe_2O_4$ under magnetic field applying.

exhibits additional benefit since it has higher magnetization compared to $ZnFe_2O_4$ (Fig. 14), thereby facilitating the magnetic separation and can be recommended as promising adsorbent for wastewater treatment.

4. Conclusion

The sol-gel auto-combustion route with the use of new mixture of fuels has been successfully proposed for the synthesis of single nanocrystalline Mg–Zn ferrite phases. The estimated crystallite size and microstrain confirm a deformation of the crystal lattice. The removal of anionic dye Congo red by $Mg_{1-x}Zn_xFe_2O_4$ ferrite samples was investigated in order to examine the impact of magnesium substitution by Zn ion in the spinel structure on adsorption activity. The adsorption isotherms for Congo red dye have been obtained. The experimental adsorption data are fitted using Langmuir, Freindlich, and Dubinin-Radushkevich isotherm models and the parameters of these models are determined. The results indicate that the Langmuir model fitted the equilibrium adsorption data better than Freindlich model, confirming the homogenous nature of the adsorbents surface-active centers. The Dubinin-Radushkevich model has been used to determine the free energy of CR adsorption on the studied samples. It is established that the mechanism of CR adsorption process onto ferrite surfaces varies from physical through ion-exchange to chemical nature with the increase of Zn content. The adsorption study of CR reveals that the studied Mg–Zn ferrospinels can be considered as good adsorbents and the proposed new synthesis method is promising, so such cation-substituted magnetic sorbents can be used for wastewater purification. It should also be noted, that the difference in the values of CR adsorption for the studied spinels is of great practical importance for future research work related to new ferrospinel compositions, as well as for modifying the synthesis methods in order to achieve enhanced adsorption capacity and selectivity.

Declaration of competing interest

The authors declare that they have no known competing financial interests or personal relationships that could have appeared to influence the work reported in this paper.

Acknowledgements

This research project is financially supported by the Ministry of Education and Science of Ukraine (Project number MESU 0117U002408 and 0118U000258). The authors are very thankful.

References

[1] T. Tatarchuk, M. Bououdina, J. Judith Vijaya, L. John Kennedy, Spinel ferrite nanoparticles: synthesis, crystal structure, properties, and perspective applications, in: O. Fesenko, L. Yatsenko (Eds.), Nanophysics, Nanomater. Interface Stud. Appl. NANO 2016. Springer Proc. Phys., Springer, Cham, 2017, pp. 305–325, https://doi.org/10.1007/978-3-319-56422-7_25.
[2] N. Ghazi, H. Mahmoudi Chenari, F.E. Ghodsi, Electrodeposition, morphology analysis, optical and magnetic properties of magnesium-zinc ferrite nanosheets, J. Magn. Magn. Mater. 468 (2018) 132–140, https://doi.org/10.1016/j.jmmm.2018.07.064.
[3] K. Kombaiah, J.J. Vijaya, L.J. Kennedy, M. Bououdina, R. Al Najar, Self heating efficiency of $CoFe_2O_4$ nanoparticles: a comparative investigation on the conventional and microwave combustion method, J. Alloy. Comp. 735 (2018) 1536–1545, https://doi.org/10.1016/j.jallcom.2017.11.278.
[4] S.M. Patil, A.M. Pawar, S.R. Thorat, B.P. Ladgaonkar, Investigation of magnesium substituted nano particle zinc ferrites for relative humidity sensors, Sens. Actuators A Phys. 244 (2016) 35–43, https://doi.org/10.1016/j.sna.2016.04.054.
[5] K. Wu, J. Li, C. Zhang, Zinc ferrite-based gas sensors: a review, Ceram. Int. 45 (2019) 11145–11157, https://doi.org/10.1016/j.ceramint.2019.03.086.
[6] K.K. Kefeni, T.A.M. Msagati, B.B. Mamba, Ferrite nanoparticles: synthesis, characterisation and applications in electronic device, Mater. Sci. Eng. B 215 (2017) 37–55, https://doi.org/10.1016/j.mseb.2016.11.002.
[7] R.I. Kharisov, H.V.R. Dias, O.V. Kharissova, Mini-review: ferrite nanoparticles in the catalysis, Arab. J. Chem. (2014), https://doi.org/10.1016/j.arabjc.2014.11.049.
[8] K.K. Kefeni, B.B. Mamba, T.A.M. Msagati, Application of spinel ferrite nanoparticles in water and wastewater treatment: a review, Separ. Purif. Technol. 188 (2017) 399–422, https://doi.org/10.1016/j.seppur.2017.07.015.
[9] M. Arruebo, M. Salazar-Alvarez, A. Abbott, Magnetic nanocarriers: evolution of spinel ferrites for medical applications, Adv. Colloid Interface Sci. 265 (2019) 29–44, https://doi.org/10.1016/j.cis.2018.01.005.
[10] N. Chubykalo, Z. Merali-Shoeli, Enzyme mimetic activities of spinel substituted nanoferrites (MFe_2O_4): a review of synthesis, mechanism and potential applications, Mater. Sci. Eng. C 98 (2019) 1424–1447, https://doi.org/10.1016/j.msec.2019.02.086.
[11] X. Hou, X. Wang, H. Mi, Progress in Fe_3O_4-based multiferroic heterostructures, J. Alloy. Comp. 765 (2018) 1127–1138, https://doi.org/10.1016/j.jallcom.2018.06.267.
[12] P. Kharbanda, T. Madaan, I. Sharma, S. Vashishtha, P. Kumar, A. Chauhan, S. Mittal, J.S. Bangruwa, V. Verma, Ferrites: magnetic materials as an alternate source of green electrical energy, Heliyon 5 (2019), e01131, https://doi.org/10.1016/j.heliyon.2019.e01131.
[13] Q. Liu, Y. He, J. Liu, F. Yang, L. Wang, J. Dong, Structural and magnetic studies of Mg substituted cobalt composite oxide catalyst $Co_{1-x}Mg_xFe_2O_4$, J. Magn. Magn. Mater. 469 (2019) 89–94, https://doi.org/10.1016/j.jmmm.2018.08.056.
[14] T. Tatarchuk, B. Al-Najar, M. Bououdina, M.A. Ait Ahmed, Catalytic and photocatalytic properties of oxide spinels, in: L. Martinez, O. Kharissova, B. Kharisov (Eds.), Handb. Ecomater., Springer, Cham, 2019, pp. 1781–1758, https://doi.org/10.1007/978-3-319-68255-6_156.
[15] T.R. Tatarchuk, M. Bououdina, N.D. Paliychuk, I.P. Yaremiy, V.V. Moklyak, Structural characterization and antistructure modeling of cobalt-substituted zinc ferrites, J. Alloy. Compd. 694 (2017) 777–791, https://doi.org/10.1016/j.jallcom.2016.10.067.
[16] T.R. Tatarchuk, N.D. Paliychuk, M. Bououdina, B. Al-Najar, M. Pacia, W. Macyk, A. Shyichuk, Effect of cobalt substitution on structural, elastic, magnetic and optical properties of zinc ferrite nanoparticles, J. Alloy. Comp. 731 (2018) 1256–1268, https://doi.org/10.1016/j.jallcom.2017.10.163.
[17] M.A. Ahmed, H.E. Hassan, M.M. Eltabey, E. Lotfa, T.R. Tatarchuk, Mössbauer spectroscopy of $Mg_xCu_{1-x}Zn_{0.5}Fe_2O_4$ (x = 0.0, 0.2 and 0.5) ferrites system irradiated by γ-rays, Phys. B Condens. Matter 530 (2017) 195–206, https://doi.org/10.1016/j.physb.2017.10.125.
[18] A. Abo El-Naga, A.M. Hassan, M.H. Mahmoud, T. Tatarchuk, I.P. Yaremiy, A.M. Gharahsoo, M.A. Ahmed, Synthesis and magnetic properties of spinel $Zn_{1-x}Ni_xFe_2O_4$ (0.0 < x < 1.0) nanoparticles synthesized by microwave combustion method, J. Magn. Magn. Mater. 471 (2019) 192–198, https://doi.org/10.1016/j.jmmm.2018.09.074.
[19] T. Tatarchuk, M. Lianbovska, V. Korzhynskyy, M. Bououdina, Green synthesis of cobalt ferrite nanoparticles using Cydonia oblonga extract: structural and mössbauer studies, Mol. Cryst. Liq. Cryst. 672 (2018) 54–66, https://doi.org/10.1080/15421406.2018.1542307.
[20] S. He, C. Lei, Q. Lai, J. Dong, Y. Fu, L. Wang, Mössbauer and structural properties of La-substituted $Ni_{0.4}Cu_{0.2}Zn_{0.4}Fe_2O_4$ nanocrystalline ferrite, Sci. Adv. Mater. 7 (2015) 1809–1815, https://doi.org/10.1166/sam.2015.2284.

Contents lists available at ScienceDirect

Chemosphere

journal homepage: www.elsevier.com/locate/chemosphere

Cobalt ferrite as an electromagnetically boosted metal oxide hetero-Fenton catalyst for water treatment

Tetiana Tatarchuk [a,b,*], Alexander Shyichuk [b,c], Nazarii Danyliuk [b], Mu. Naushad [d], Volodymyr Kotsyubynsky [e], Volodymyra Boychuk [e]

[a] Faculty of Chemistry, Jagiellonian University, 30-387, Kraków, Poland
[b] Educational and Scientific Center of Material Science and Nanotechnology, Vasyl Stefanyk Precarpathian National University, Ivano-Frankivsk, 76018, Ukraine
[c] Faculty of Chemical Technology and Engineering, Bydgoszcz University of Science and Technology, 85-326, Bydgoszcz, Poland
[d] Department of Chemistry, College of Science, King Saud University, P.O. Box 2455, Riyadh, 11451, Saudi Arabia
[e] Department of Material Science and New Technology, Vasyl Stefanyk Precarpathian National University, 76018, Ivano-Frankivsk, Ukraine

HIGHLIGHTS

- Electromagnetic heating is used to boost the catalytic activity of cobalt ferrite.
- The reaction order increases with increasing H_2O_2 concentration.
- Induction heating accelerates the catalytic decomposition of H_2O_2 up to 2 times.
- Induction heating accelerates the Fenton-like oxidation of caffeine more than 2 times.
- Electromagnetically heated $CoFe_2O_4$ can

GRAPHICAL ABSTRACT

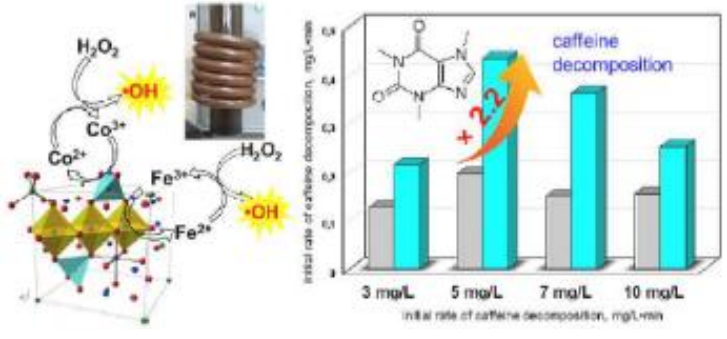

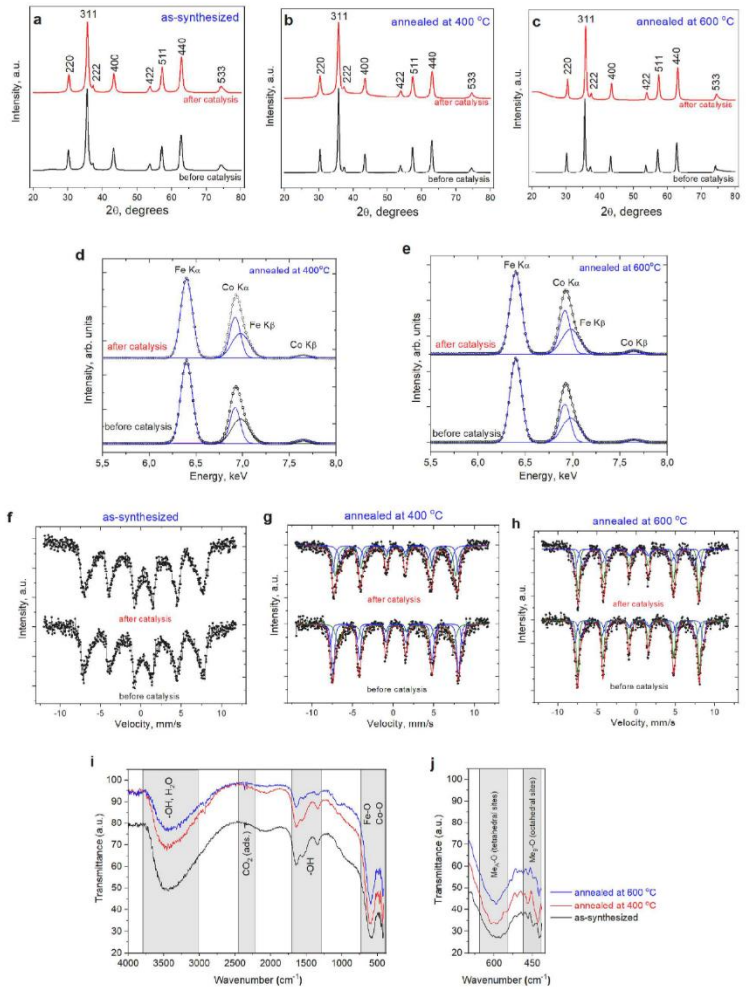

Fig. 1. XRD patterns of the $CoFe_2O_4$ samples: (a) as-synthesized $CoFe_2O_4$, (b) $CoFe_2O_4$ annealed at 400 °C, and (c) $CoFe_2O_4$ annealed at 600 °C. Deconvoluted XRF spectra of the $CoFe_2O_4$ samples annealed at 400 °C (d) 600 °C (c) before and after catalysis. (f,g,h) Mössbauer spectra of the $CoFe_2O_4$ samples, with blue lines marking the sub-spectra corresponding to Fe^{3+} ions located in A and B crystal sites. (g) The full FTIR spectra of $CoFe_2O_4$ (as-synthesized, annealed at 400 and 600 °C), and (h) the spectral range inherent to Me–O bonds vibrations in the spinel crystal lattice. (For interpretation of the references to colour in this figure legend, the reader is referred to the Web version of this article.)

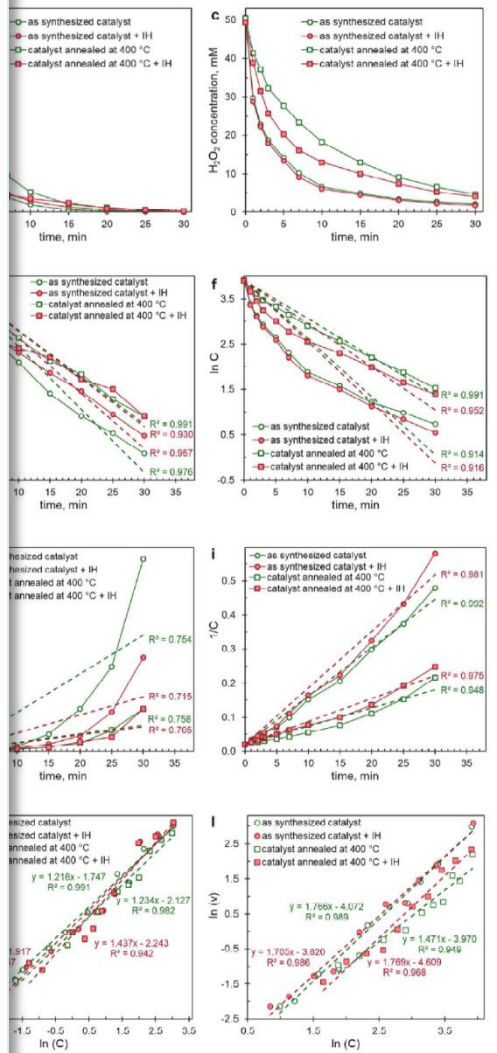

concentrations, and the same data plotted in coordinates of different kinetic models: (d,e,f) l power law model. The initial H_2O_2 concentration is: (a,d,g,j) 5 mM, (b,e,h,k) 20 mM, (c,f,i, /L. The use of magnetic induction heating is indicated in the legends. $V(H_2O_2)$ = 100 mL.

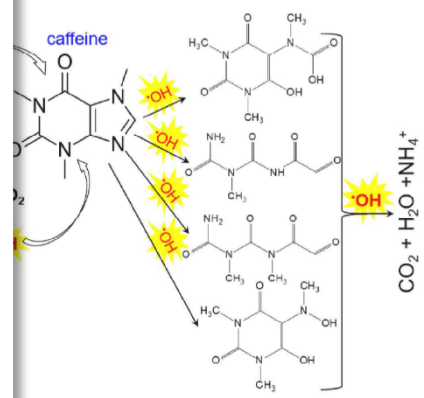

ated caffeine degradation using hetero-Fenton cobalt ferrite catalyst.

(11)

11) , the
ases. The
and (11)

re of the
e catalyst
arameters
of the as-
ize of the
Probably,
rface. The
reduced
ent with a
tant after
raction of
nt on the

on heating
n heating
nealed at
ubsequent
orption of
dition of
e. At the
mposition
ration in-
indicates
decompo-
caffeine
of 3 mg/
nding on
heating.
from 1.6

the reac-
mposition
creases as

the initial concentration of caffeine increases (Fig. 4c). When the electromagnetic field is applied, the decomposition reaction accelerates significantly (Fig. 4c). The initial rate of the decomposition of H_2O_2 increases from 1.1 to 2 times (Fig. 4d). Fig. 4e shows kinetic lines of the adsorption/degradation of caffeine with induction heating. Initial reagents concentrations have a clear effect on the rate of caffeine degradation. As the H_2O_2 concentration increases, the initial rate of caffeine decomposition increases monotonically (Fig. 4f). On the other hand, the concentration of caffeine has a non-monotonic effect. Initially, an increase in the initial concentration of caffeine results in an increase in the rate of caffeine decomposition (Fig. 4f). However, a further increase in the initial concentration of caffeine above 5 mg/L inhibits the reaction rate (Fig. 4f). This effect can be explained by the multi-stage nature of the studied reaction. The caffeine molecule easily gives up the hydrogen atom from its imidazole ring to a hydroxyl radical (Jia et al., 2021; Torun et al., 2014; Ziylan-Yavas et al., 2021). However, a deep breakdown of the molecular structure of caffeine only occurs after further radical attacks. Too much caffeine reduces the number of radicals available for the subsequent degradation steps. In this way, the molecular structure of caffeine breaks down more slowly. Fig. 4g and h shows the effect of the initial concentrations of the reagents on their final decomposition degrees under induction heating. The observed increase in the degree of caffeine decomposition with increasing H_2O_2 concentration and decreasing caffeine concentration (Fig. 4g) is quite obvious. Interestingly, changes in the degree of decomposition of H_2O_2 depending on the initial concentrations of H_2O_2 and caffeine have exactly the same trends (Fig. 4h). Both effects can be explained by taking into account the side reactions (9)-(11). The decrease in the degree of decomposition of H_2O_2 with the initial concentration of caffeine is due to the scavenging of radicals by caffeine. The result is the inhibiton of reaction (9) and a decrease in the overall degree of hydrogen peroxide decomposition. On contrary, the increase in the initial concentration of H_2O_2 accelerates the reaction (9). The result is an increase in the undesirable reaction (11) and an increase in the overall degree of H_2O_2 decomposition. The main intermediates, which can be formed during the Fenton oxidation, are shown in Fig. 5 (Jia et al., 2021; Torun et al., 2014; Ziylan-Yavas et al., 2021). They are formed due to attack of imidazole ring by free radicals. These organic compounds can further react with hydroxyl radicals, eventually leading to full mineralization.

metals cations distribution. Ceram. Int. 47, 19234–19240. https://doi.org/10.1016/j.ceramint.2021.03.149.
Almind, M.R., Vendelbo, S.B., Hansen, M.F., Vinum, M.G., Frandsen, C., Mortensen, P. M., Engbæk, J.S., 2020. Improving performance of induction-heated steam methane reforming. Catal. Today 342, 13–20. https://doi.org/10.1016/j.cattod.2019.05.005.
Almind, M.R., Vinum, M.G., Wismann, S.T., Hansen, M.F., Vendelbo, S.B., Engbæk, J.S., Mortensen, P.M., Chorkendorff, I., Frandsen, C., 2021. Optimized CoNi nanoparticle composition for curie-temperature-controlled induction-heated catalysis. ACS Appl. Nano Mater. 4, 11537–11544. https://doi.org/10.1021/acsanm.1c01941.
Alzoubi, G.M., Albiss, B.A., Shatnawi, M., Bsoul, I., Alsmadi, A.M., Salameh, B., Alna'washi, G.A., 2020. Influence of high-temperature annealing on structural and magnetic properties of crystalline cobalt ferrite nanoparticles in the single-domain regime. J. Supercond. Nov. Magnetism 33, 3179–3188. https://doi.org/10.1007/s10948-020-05551-w.
Anantharamaiah, P.N., Rao, P., Shashanka, H.M., Khopkar, V., Arout Chelvane, J., Sahoo, B., Ramana, C.V., 2022. Tunable dielectric properties of nickel ferrite derived via crystallographic site preferential cation substitution. J. Phys. Chem. C 126, 9123–9134. https://doi.org/10.1021/acs.jpcc.2c00529.
Anastopoulos, I., Pashalidis, I., Orfanos, A.G., Manariotis, I.D., Tatarchuk, T., Sellaoui, L., Bonilla-Petriciolet, A., Mittal, A., Núñez-Delgado, A., 2020. Removal of caffeine, nicotine and amoxicillin from (waste)waters by various adsorbents. A review. J. Environ. Manag. 261, 110236 https://doi.org/10.1016/j.jenvman.2020.110236.
Ati, A.A., Abdalsalam, A.H., Hasan, A.S., 2021. Thermal, microstructural and magnetic properties of manganese substitution cobalt ferrite prepared via co-precipitation method. J. Mater. Sci. Mater. Electron. 32, 3019–3037. https://doi.org/10.1007/s10854-020-05053-4.
Banerjee, A.M., Pai, M.R., Meena, S.S., Tripathi, A.K., Bharadwaj, S.R., 2011. Catalytic activities of cobalt, nickel and copper ferrospinels for sulfuric acid decomposition: the high temperature step in the sulfur based thermochemical water splitting cycles. Int. J. Hydrogen Energy 36, 4768–4780. https://doi.org/10.1016/j.ijhydene.2011.01.073.
Bayerl, T., Duhovic, M., Mitschang, P., Bhattacharyya, D., 2014. The heating of polymer composites by electromagnetic induction – a review. Compos. Part A Appl. Sci. Manuf. 57, 27–40. https://doi.org/10.1016/j.compositesa.2013.10.024.
Bokare, A.D., Choi, W., 2014. Review of iron-free Fenton-like systems for activating H2O2 in advanced oxidation processes. J. Hazard Mater. https://doi.org/10.1016/j.jhazmat.2014.04.054. Journal of Hazardous Materials.
Bordet, Alexis, Lacroix, L.-M., Fazzini, P.-F., Carrey, J., Soulantica, K., Chaudret, B., 2016. Magnetically induced continuous CO2 hydrogenation using composite iron carbide nanoparticles of exceptionally high heating power. Angew. Chem. 128, 16126–16130.
Cerezo-Navarrete, C., Marín, I.M., García-Miquel, H., Corma, A., Chaudret, B., Martínez-Prieto, L.M., 2022. Magnetically induced catalytic reduction of biomass-derived oxygenated compounds in water. ACS Catal. 12, 8462–8475. https://doi.org/10.1021/acscatal.2c01696.
Dhaka, S., Kumar, S., Poonia, K., Singh, V., Dhaka, K., Mund, H.S., 2021. Effect of annealing temperature on structural and magnetic properties of nano-cobalt ferrite. J. Mater. Sci. Mater. Electron. 32, 16392–16399. https://doi.org/10.1007/s10854-021-06192-y.
Dihingia, H., Tiwari, D., 2022. Impact and implications of nanocatalyst in the Fenton-like processes for remediation of aquatic environment contaminated with micro-pollutants: a critical review. J. Water Process Eng. 45, 102500.
Dong, C., Fang, W., Yi, Q., Zhang, J., 2022. A comprehensive review on reactive oxygen species (ROS) in advanced oxidation processes (AOPs). Chemosphere 308, 136205. https://doi.org/10.1016/j.chemosphere.2022.136205.
Fache, A., Marias, F., 2020. Dynamic operation of fixed-bed methanation reactors: yield control by catalyst dilution profile and magnetic induction. Renew. Energy 151, 865–886. https://doi.org/10.1016/j.renene.2019.11.081.
Fache, A., Marias, F., Chaudret, B., 2020. Catalytic reactors for highly exothermic reactions: steady-state stability enhancement by magnetic induction. Chem. Eng. J. 390, 124531 https://doi.org/10.1016/j.cej.2020.124531.
Fu, W., Yi, J., Cheng, M., Liu, Y., Zhang, G., Li, L., Du, L., Li, B., Wang, G., Yang, X., 2022. When bimetallic oxides and their complexes meet Fenton-like process. J. Hazard Mater. 424, 127419.
Gallo-Cordova, A., Castro, J.J., Winkler, E.L., Lima, E., Zysler, R.D., Morales, M., del, P., Ovejero, J.G., Streitwieser, D.A., 2021. Improving degradation of real wastewaters with self-heating magnetic nanocatalysts. J. Clean. Prod. 308, 127385 https://doi.org/10.1016/j.jclepro.2021.127385.
Ghosh, M.P., Mukherjee, S., 2019. Microstructural, magnetic, and hyperfine characterizations of Cu-doped cobalt ferrite nanoparticles. J. Am. Ceram. Soc. 102, 7509–7520. https://doi.org/10.1111/jace.16687.
Guan, R., Yuan, X., Wu, Z., Jiang, L., Li, Y., Zeng, G., 2018. Principle and application of hydrogen peroxide based advanced oxidation processes in activated sludge treatment: a review. Chem. Eng. J. 339, 519–530. https://doi.org/10.1016/j.cej.2018.01.153.
Gupta, M., Das, A., Dutta, S., Mohapatra, S., Datta, A., 2022. Magnetic and mössbauer study of lanthanum doped nanosized cobalt ferrite assembly. SSRN Electron. J. https://doi.org/10.2139/ssrn.4085275.
Gyergyek, S., Lisjak, D., Beković, M., Grilc, M., Likozar, B., Nečemer, M., Makovec, D., 2020. Magnetic Heating of Nanoparticles Applied in the Synthesis of a Magnetically Recyclable Hydrogenation Nanocatalyst, vol. 10. https://doi.org/10.3390/nano10061142.
Han, M., Wang, H., Jin, W., Chu, W., Xu, Z., 2022. The performance and mechanism of iron-mediated chemical oxidation: advances in hydrogen peroxide, persulfate and percarbonate oxidation. J. Environ. Sci. https://doi.org/10.1016/j.jes.2022.07.037.

первинні джерела:
статті, патенти, дисертації, доповіді конф.
безпосередній опис результатів

вторинні джерела
(огляди, монографії,
енциклопедії, підручники):
узагальнення результатів

третинні джерела
(бази даних):
стисле викладення + пошук

metals

MDPI

Article

Green Synthesis of Cobalt–Zinc Ferrites and Their Activity in Dye Elimination via Adsorption and Catalytic Wet Peroxide Oxidation

Mariia Liaskovska [1,2], Tetiana Tatarchuk [3,4,*] and Volodymyr Kotsyubynsky [5]

1 Department of Chemistry, Vasyl Stefanyk Precarpathian National University, 76018 Ivano-Frankivsk, Ukraine; liaskovskam@gmail.com or mliaskovska@ifnmu.edu.ua
2 Department of Biological and Medical Chemistry, Ivano-Frankivsk National Medical University, 76018 Ivano-Frankivsk, Ukraine
3 Faculty of Chemistry, Jagiellonian University, 30-387 Kraków, Poland
4 Educational and Scientific Center of Materials Science and Nanotechnology, Vasyl Stefanyk Precarpathian National University, 76018 Ivano-Frankivsk, Ukraine
5 Department of Materials Science and New Technologies, Vasyl Stefanyk Precarpathian National University,

nanomaterials

MDPI

Review

Studying the Defects in Spinel Compounds: Discovery, Formation Mechanisms, Classification, and Influence on Catalytic Properties

Tetiana Tatarchuk [1,2]

[1] Faculty of Chemistry, Jagiellonian University, ul. Gronostajowa 2, 30-387 Kraków, Poland; tatarchuk.tetyana@gmail.com

[2] Educational and Scientific Center of Materials Science and Nanotechnology, Vasyl Stefanyk Precarpathian National University, 76018 Ivano-Frankivsk, Ukraine

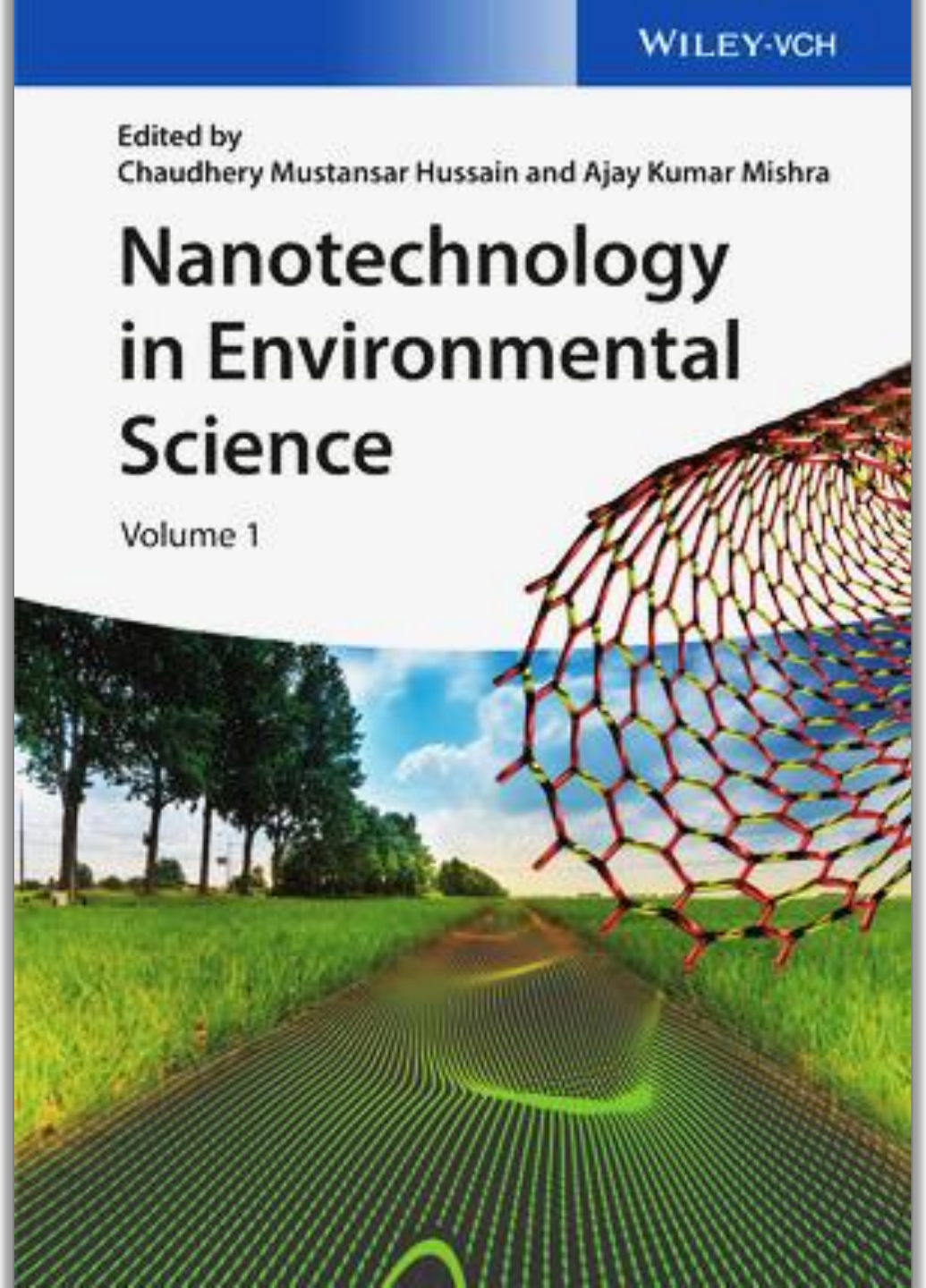

8

Photocatalysis: Activity of Nanomaterials

Tetiana Tatarchuk,[1] Amalthi Peter,[2] Basma Al-Najar,[3] Judith Vijaya,[2] and Mohamed Bououdina[3]

[1]*Vasyl Stefanyk Precarpathian National University, Department of Theoretical and Applied Chemistry, 57, Shevchenko Str., Ivano-Frankivsk 76018, Ukraine*
[2]*Loyola College, Department of Chemistry, Catalysis and Nanomaterials Research Laboratory, Nelson Manickam Road, Chennai, Tamil Nadu 600034, India*
[3]*University of Bahrain, Department of Physics, PO Box 32038, Sakhir, Kingdom of Bahrain*

8.1 Nanomaterials for Photocatalysis

In the past few years, nanomaterials have emerged as one of the main influencers in technology and biomedicine. The extremely small size of nanomaterials (5–100 nm) owe them miraculous properties due to their large surface area in addition to quantum confinement. It is well known that nanomaterials can be shaped in many forms as rods, thin films, powder, and so on [1,2]. They also can be synthesized through several methods resulting in different shapes, sizes, and properties [3]. Therefore, they are applied in mostly every life sector including drugs and modifications, manufacturing, and materials, environmental issues, electronics, energy production, and industry [4]. The photocatalysis process using the unique properties of nanomaterials has been applied in a wide range of applications such as degradation of pollutants from atmosphere and water. It is also used in producing energy. Some nanomaterials such as oxides [5–7], semiconductors [8,9], metals [10,11], and graphene [12,13] have shown great effect on photocatalysis processes [14,15] due to their enhanced and controllable optical properties, which makes them excellent photocatalysts. This chapter will discuss the mechanism of photocatalysis processes using nanomaterials and their applications. Table 8.1 shows some of the nanoparticles applied for photocatalytics procedures. The chapter will also focus on the different types of nanomaterials used in photocatalysis in terms of their synthesis method, microstructure, and their optical and magnetic properties.

Nanotechnology in Environmental Science, First Edition. Edited by Chaudhery Mustansar Hussain and Ajay Kumar Mishra.

Іванна ЛАПЧУК
Олександр ШИЙЧУК
Тетяна ТАТАРЧУК

БІОЦИДНІ ПОВЕРХНІ:
інженерія, механізм дії та застосування




УКРАЇНА

ПАТЕНТ

НА КОРИСНУ МОДЕЛЬ

№ 153459

СПОСІБ ОТРИМАННЯ КОБАЛЬТ-ФЕРИТНОГО ГРАНУЛЬОВАНОГО КАТАЛІЗАТОРА РОЗКЛАДУ ПЕРОКСИДУ ВОДНЮ

Видано відповідно до Закону України "Про охорону прав на винаходи і корисні моделі".

Зареєстровано в Державному реєстрі України корисних моделей **12.07.2023.**

В.о. директора
Державної організації «Український національний офіс інтелектуальної власності та інновацій» І.В. Паренчук

УКРНОІВІ

УКРАЇНА

ПАТЕНТ

НА КОРИСНУ МОДЕЛЬ

№ 152724

СПОСІБ ОТРИМАННЯ ГРАНУЛЬОВАНОГО КАТАЛІЗАТОРА ДЛЯ ДЕЗІНФЕКЦІЇ ВОДИ

Видано відповідно до Закону України "Про охорону прав на винаходи і корисні моделі".

Зареєстровано в Державному реєстрі України корисних моделей **05.04.2023.**

Директор
Державної організації «Український національний офіс інтелектуальної власності та інновацій» О.П. Орлюк

УКРНОІВІ